Chapter 6. Physical and chemical properties of van der Waals interfaces

In this chapter, interfaces of layered semiconductors are studied in terms of chemical and electrical properties. Section 6-1 is a brief review on the metal-semiconductor interface and surface/interface photovoltaic effects. In section 6-2, the growth of a layered material $SnSe_2$ on various substrates is reported. It was found that $SnSe_2$ is epitaxially grown at the lowest substrate temperature (~230°C) ever known for VDWE of layered materials. The epitaxial growth was achieved on various layered materials (MoS_2, $NbSe_2$, graphite), while reaction took place with Al_2O_3(0001) substrates. The observed band bending was consistent with the work function difference between the film and the substrate, indicating the Schottky limit property of the junctions.

In section 6-3, the photovoltaic effect at van der Waals metal-semiconductor interfaces is studied by XPS. It was found that the value of photovoltage at low temperature is equal to the amount of band bending. It verifies the expectation that no Fermi level pinning occurs at the van der Waals interfaces.

6-1. Metal-semiconductor interfaces

Interfaces of semiconductors play essential roles in electronic devices [1]. In particular, metal-semiconductor interfaces are important in some microwave and photoelectric devices, and in electrodes connecting semiconductor devices with outside. Although various approaches have been taken to understand the properties of metal-semiconductor interfaces, the history of the study is filled with incessant disputes about model theories and new phenomena until now [2].

There are various kinds of electric properties in metal-semiconductor interfaces. Figure 6-1-1 illustrates the electronic properties of the metal-semiconductor interfaces. The "linear model" of Schottky barrier formation is often applicable to a junction between a range of metals of work function ϕ_m and a given semiconductor of electron affinity χ_{sc}. According to the model, the barrier height ϕ_b is given by $\phi_b = S(\phi_m - \chi_{sc}) + C$, where S is a parameter characteristic to the interface and C is a constant. For the case of complete pinning of the Fermi level by surface or interface state, S=0, whereas in the Schottky limit with no such pinning, S=1. Schottky limit property, S=1, is achieved when the following criteria are satisfied. (a) The band gap of the semiconductor must be large enough to enable the Fermi level to shift by $\phi_m - \chi_{sc}$. (b) The semiconductor surface must be free from intrinsic surface states in the fundamental band gap. (c) The metal and the semiconductor should not react chemically or intermix with each other. Besides these classical views, theories involving quantum effects is proposed. Metal induced gap states (MIGS) theory [3] is one of those, in which mid-gap states are formed by the evanescent wave function exuding from the metal into the semiconductor. The occurrence of such effects have not been confirmed yet, and it is expected that it will be observed only when the density of other mid-gap states due to reactions and surface states are negligible.

Material combinations of two layered metal chalcogenides, one material grown epitaxially on top of each other, have attractive features in this regard.

Firstly, the layered metal dichalcogenides have unique structures characterized by chalcogen-metal-chalcogen sandwiches which are held together by van der Waals forces. Secondly, changing the combination of metal and chalcogen, it is possible to obtain ranging value of the band gap and work function, from nearly insulating HfS_2 to metallic $NbSe_2$ and from 4.1 eV of $MoTe_2$ to 5.3 eV of $SnSe_2$, respectively. Thirdly, the intrinsic surface states resulting from the terminated translational symmetry of the crystal do not exist on semiconducting metal dichalcogenides surfaces, since the outer surfaces are chemically saturated by chalcogen atoms, forming van der Waals surfaces. Lastly, recently developed VDWE can fabricate atomically abrupt and chemically inert interfaces of two adjacent metal dichalcogenides of almost all combinations. A proper selection of these material systems, therefore, will fulfill the above criteria and allow the study of ideal Schottky interfaces. Although there have been several report on the fabrication of p-n junctions by layered semiconductor $MoSe_2$ and WSe_2 [4], studies on the layered metal-semiconductor systems have not been reported. In section 6-2, the band-offset in the layered material systems is studied by using VDWE of $SnSe_2$, a layered semiconductor.

Much interest has been recently focused on the measurement of the Schottky barrier height by photoemission techniques, where the incident photons induce not only photoelectron emission but also produce electron-hole pairs within the semiconductor surface space-charge region that are separated by the electric field, resulting in a reduction of the band bending [5]. For n-type band bending, electrons move away from the surface while minority holes move toward the metal, acting to reduce this internal electric field, as a result of producing an "open circuit" voltage, or a surface photovoltage. While this effect is small at room temperature, it can be as large as the build-in band bending at low temperatures because the leak current due to the recombination with thermally activated carriers is reduced. It is therefore useful to utilize this "dynamic" effect for characterization of the Schottky behavior at the metal-

semiconductor interfaces. This effect is studied in interfaces of layered materials in section 6-3.

6-2. Molecular beam epitaxy of $SnSe_2$: Chemistry and electronic properties of interfaces

6-2-1 Introduction

$SnSe_2$ is a semiconductor with a hexagonal layered structure and an indirect band gap of 1.1 eV. It is known to exhibit interesting electronic and optical properties, which may lead to unique applications. The layered structure and high optical absorbance of $SnSe_2$ make it suitable for solar cells [6]. Memory effects in electronic switching at $SnSe_2$-metal interfaces have been reported [7]. Multilayering with a relative compound SnS_2 is also considered as an optical waveguide in which the high second-harmonic generation coefficient of SnS_2 [8] is useful in these applications. In all of these applications it is considered that a high degree of crystallinity is important in achieving desired functions and properties. In particular, quantum optic application requires single crystals, or at least highly aligned microcrystals. Thin films of $SnSe_2$ with right stoichiometry have been fabricated on glasses or single crystals of sodium chloride by several groups [6], but they are not single-domain single crystals, i.e., microcrystalline films aligned only along the c-axis. A recent effort of molecular beam epitaxy (MBE) of layered materials, called van der Waals epitaxy [9], has enabled complete epitaxial growth of layered materials, in which excellent crystallinity of the grown thin films is achieved due to the inactive surface of the substrates and the symmetry coincidence between the film and the substrate. This section reports the MBE growth and electronic property of $SnSe_2$ films grown on layered materials. The phase diagram of the Sn-Se system in thin films is also studied. The grown films were characterized by means of x-ray photoelectron spectroscopy (XPS), reflection high energy electron diffraction (RHEED), and scanning tunneling microscopy (STM). The

work function of the films was also measured using secondary electron cut-off in ultraviolet photoemission to study the electronic property of the layered hetero junction.

6-2-2 Experimental

Growth and characterization, except by STM, were all performed *in situ* under ultrahigh-vacuum (UHV) conditions. The growth chamber equipped with RHEED was pumped by a turbo molecular pump to a base pressure of 2×10^{-7} Pa. A molecular beam of tin was sublimed from molten metallic tin (99.995%) heated on a Mo heater. For the selenium source, a unique method described below was used. $SnSe_2$ decomposes to emit selenium vapor at 340-400°C, which is higher than the temperature during bake-out of conventional vacuum systems. We have utilized this decomposition reaction for the selenium source (chapter 10) [10]. $SnSe_2$ crystals grown by the Bridgman method were placed in a Pyrex glass cell heated to around these temperatures to produce Se vapor. Vapor pressure of the selenium during the growth was 2×10^{-5} Pa.

I have attempted growth on various substrate materials with different electronic properties: semiconducting MoS_2, metallic $NbSe_2$, semi-metallic highly oriented pyrolytic graphite (HOPG), and insulating $Al_2O_3(0001)$, all surface symmetries of which are hexagonal. All layered material substrates, MoS_2, $NbSe_2$ and HOPG, were cleaved *in situ* by Cu foil adhesive tapes, and their respective surface crystallographies were checked by RHEED. $Al_2O_3(0001)$ was Ar^+ ion sputtered followed by annealing at 900°C in UHV using an electron bombardment heater. RHEED streak patterns were observed after annealing for 10 min.

The substrates were heated by a Mo wire heater to various temperatures during and after the growth. A mechanical shutter located about 1 cm below the substrate was used to control the molecular beams. Thin film growth was monitored by RHEED with an acceleration energy of 20kV, along with a quartz

oscillator for the growth rate. After the growth, the specimens were subsequently transferred to analysis chambers which were ion-pumped to base pressures of 3×10^{-8} Pa. XPS was performed by means of the ESCA-100 system (Surface Science Laboratory) with the energy resolution of 0.8eV in FWHM calibrated with $Au(4f_{7/2})$. Work functions were measured by the angle resolved spectrometer ARIES HAC-300(VSW) with a He-I discharge lamp (photon energy $h\nu$=21.2eV) [11]. STM was carried out in ambient atmosphere after the films were taken out from the UHV system. Digital Instruments' Nanoscope II with W tips was used.

6-2-3 Results

A. Growth on MoS_2 substrates

First let us describe the growth on MoS_2 at various substrate temperatures. As growth started at 200-220°C, the RHEED streak pattern of the substrate (lattice constant 3.16Å) decayed gradually, and a new streak pattern appeared in a few minutes. It had hexagonal symmetry around the c-axis and was aligned with the substrate. From the spacing of streaks the lattice constant along the a-axis of the films was found to be 3.75±0.10Å, which is consistent with the bulk value (3.81Å). In Fig. 6-2-1 the XPS valence band spectrum of a thick film is compared with that of the bulk single-crystal $SnSe_2$. In these identical spectra, there are 0.9 eV gaps below the Fermi level, which indicates the film as well as the bulk were n-type. The binding energies and peak ratio of core levels are also equal to those of the bulk. Surface morphology was also studied by means of STM (Fig. 6-2-2). Figure 6-2-2(a) shows an atomic image of the hexagonal lattice, the lattice constant of which was consistent with the bulk value. After the tip was scanned over the sample surface several times, the surface was etched layer by layer, as shown in Fig. 6-2-2(b). The height of the steps, measured from the histogram, was about 6Å which is consistent with the bulk value (6.14Å). In order to elucidate the stoichiometry-temperature

relationship, the Sn($3d_{5/2}$) and Se(3d) core level spectra from thick films (>500 Å) grown at various temperatures were examined. At higher than 220°C, Se-deficient films are formed. In addition, Sn($3d_{5/2}$) core levels are shifted to lower binding energy and RHEED streak patterns are faded or sometimes totally absent. In particular, films grown at around 350°C show compositions which have binding energies corresponding to SnSe. The growth rate decreases significantly above 500°C, and no tin was detected by XPS from the sample treated at 550°C; instead selenium was detected, indicating the substitution of Se into MoS_2 as MoS_xSe_{2-x} (Fig. 6-2-3). In this case, the RHEED streak pattern was still observable, but much weaker. In a control experiment, the MoS_2 substrate was heated to 550°C under the same Se vapor pressure for the same duration of time. However, Se was not detected by XPS. It is therefore suggested that tin catalyzes the exchange reaction of Se and S of MoS_2.

$SnSe_2$ epitaxial films were also formed by deposition of tin followed by annealing under selenium vapor. Deposition of Sn to MoS_2 only showed a halo or ring RHEED pattern, depending on the amount of tin deposited. Streak patterns consistent to $SnSe_2$ appeared when the sample was annealed under the selenium vapor for long period of time at 220°C. The electron beam for RHEED is not responsible for the crystallization since it occurs even when RHEED is turned off during the annealing. For the crystallization, there are no distinction of thickness for tin although the annealing time becomes longer with larger amount of tin. Without selenium the RHEED pattern remains unchanged.

B. Substrate effects

Epitaxial growth conditions were nearly identical for other types of layered substrates, i.e., $NbSe_2$ and HOPG. RHEED from the films on $NbSe_2$ showed similar temperature dependence as described previously. While a columnar streak pattern was observed from the films grown on HOPG at 200-220°C, further information was not obtained due to the polycrystalline nature of the substrate. XPS of the films on these substrates were identical to that of the

bulk single crystal, yet different in terms of the shifts originating from band bending, which will be discussed later.

Epitaxial films were not obtained from the growth on $Al_2O_3(0001)$ substrates. The streak RHEED pattern from the substrate disappeared soon after the growth started at 220°C, and only very diffused ring patterns were observed. When tin was deposited on $Al_2O_3(0001)$ at 220°C, XPS of Sn(3d) indicated a reaction with oxygen. The sublimation of $SnSe_x$ took place at 300°C which is much lower than for $SnSe_2$ on MoS_2.

C. Band bending and work function

The binding energies of the films have shown shifts, the magnitude of which depends on the thickness. For MoS_2 substrates, the binding energy shift from the bulk core levels was observed, while $NbSe_2$ and HOPG showed no change from the bulk. These shifts are attributed to the band bending of the film or the substrate. Maximum values of these shifts are shown in Table 6-2-4. The shifts of $SnSe_2$ on $NbSe_2$ show thickness dependence, and the absolute value decreases to 0.30eV at a film thickness of about 100Å.

Since the band bending is strongly related to the work functions of the materials, those values of MoS_2, $NbSe_2$, HOPG and $SnSe_2$ single crystals and of a thick film on MoS_2 were measured using secondary electron cut-off in UPS. The details of the method are described in chapter 3. The results are shown in Table 6-2-5. The error associated with the measurement is estimated as less than ±0.1 eV from the repeated experiments for different samples of similar materials. The work function of films grown over MoS_2 was identical to that of bulk $SnSe_2$.

6-2-4 Discussion

A. Electronic structure of the epitaxial film

The energy diagrams from the observed band bending are schematically illustrated in Fig. 6-2-6. The amount of band bending is consistent with the

measured work function, within error. This suggests that there are no surface states or interface double layers in these systems. In the $SnSe_2$ / MoS_2 interfaces, only MoS_2 (n-type) has undergone band bending, indicating that the carrier concentration in $SnSe_2$ is much higher than that in MoS_2 (typically 10^{16}~10^{17} cm^{-3}). Since HOPG has a lower work function than n-type $SnSe_2$, the interface formed an Ohmic contact. The $SnSe_2$ / $NbSe_2$ system appears to be within a Schottky limit because the bending is consistent with the work function difference.

One can estimate the carrier concentration from the thickness dependence of band bending at the metal-semiconductor Schottky barrier. By assuming the depletion approximation, the carrier concentration N is a simple function of the depletion length D [2]:

$$V(x)=(N / 2\varepsilon_r\varepsilon_0)\, q\, (D-x)^2 , \qquad (6\text{-}2\text{-}1)$$

where ε_0, ε_r, and q are the dielectric constant of vacuum, the relative dielectric constant of the semiconductor, and the charge of the carrier, respectively. V(x) is the amount of band bending at position x from the interface. Although the validity of eq. (6-2-1) for films with thickness less than D is not found in the literature, eq. (6-2-1) can be used also for thin films by the following reasoning. The depth of the n-type carrier is estimated from the difference of the band gap (1.1eV) and valence band maximum in XPS (0.9eV), as 0.2 eV, which is much smaller than the band gap. Therefore the depletion approximation is valid also for the thin films and thus follows eq. (6-2-1). Here we know two values of V(x) for two extreme points from the shifts of XPS spectra: 0.55V at x~6Å (1ML) , 0.30V at x ~100Å. Then we can eliminate D and obtain N ~ 5 x 10^{17} cm^{-3}, assuming ε_r~10. This value is comparable with the reported bulk value [7], indicating the high quality of the film.

B. Applications

The present study has provided information on the applicability of this material. The low epitaxy temperature of $SnSe_2$ makes it suitable for inorganic-

organic epitaxial heterojunctions in which one can utilize a variety of electronic and optical properties of organic materials. Recent epitaxial growth of organic molecules is gathering widespread interest [12]. It is expected that $SnSe_2$ can be grown onto some of these organic systems and may be utilized as a buffer layer to prevent re-evaporation of the organics during the growth of other materials. The etching of epitaxial films by means of STM [13] may also be utilized to fabricate nanoscale patterning in inorganic-organic systems.

The fast recrystallization of the films indicates that the structure of $SnSe_2$ changes quickly in accordance with the environment. This probably accounts for unusual time- and polarity- dependent electronic properties [7]. For the application in solar cells, it was found that Schottky solar cells with n-type $SnSe_2$ will not easily be realized because of its high work function. Fabrication of p-type doped $SnSe_2$ is desired for use in a p-n junction solar cell with n-$SnSe_2$, in which one can make use of the high optical absorbance of $SnSe_2$. In this case, the p-type Schottky junction is also promising since p-$SnSe_2$ possesses an incomparably high work function as a semiconductor. The S-Se exchange reaction observed on MoS_2 at 550°C can be utilized to modify the surfaces of MoS_2 or, possibly, other layered materials. Since MoS_2 derivatives are reported to be efficient hydrogenation catalysts [14], the present finding is expected to pave the way to the fabrication of new catalytic systems.

6-2-5 Conclusions

Epitaxial films of layered $SnSe_2$ were fabricated for the first time and the temperature-stoichiometry relationship was studied. Heterojunction properties with other layered materials appear to be consistent with the work function difference (Schottky limit). The characteristics of $SnSe_2$ discovered in the present study, such as low crystallization temperature, high work function and quick etching with STM, will lead to unique applications of this material. Epitaxial films are not formed on Al_2O_3(0001) due to the reaction.

6-3. Photovoltaic properties of van der Waals interfaces

6-3-1 Introduction

By the motivation described in section 6-1, I have studied the band bending and the interface photovoltage in VDWE systems by using XPS. In the present study 2Ha-$TaSe_2$ was chosen as a metal which was grown by means of VDWE over p- or n- types of WSe_2 semiconducting substrates. 2Ha-$TaSe_2$ is known as a metal with charge density waves. Since the work function did not change within the experimental error (±0.1eV) for similar material 2Ha-TaS_2, I utilized the low growth temperature of 2Ha-$TaSe_2$ in order to prevent interface reactions which might occur at high growth temperatures. WSe_2 is a semiconductor with 0.9 eV band gap and 4.1 eV (n-type) and 5.0 eV (p-type) work functions, which is considered as a promising material for solar cells [15]. It was found that there were no band bending on the TaS_2 / p-WSe_2 system, whereas a large photovoltaic effects observed on $TaSe_2$ / n-WSe_2 system was nearly compensates the band bending of $TaSe_2$ and n-WSe_2. It was concluded that the junction does not have the Fermi level pinning.

6-3-2 Experimental

The experiments presented here were performed with n- and p- type WSe_2 single crystals grown by iodine vapor transport with stoichiometric W and Se and Nb-dopant replacing W, respectively. The sample was cleaved in UHV to expose new van der Waals surfaces, upon which $TaSe_2$(2Ha) was epitaxially grown in the growth chamber as described in chapter 4 (low temperature grown and annealed above 420°C). The deposition rate was monitored by a quartz oscillator and RHEED was used for real-time monitoring of the growth process. It was identified that the crystalline thin film of $TaSe_2$(0001) was grown on both p and n (0001) WSe_2 with their hexagonal crystal axes aligned. After growth to the desired thickness, the specimen was transferred "in-situ" to the

characterization chamber, where the photoemission (XPS) measurement with a monochromatized Al-Kα x-ray was performed. The resolution achieved for Au($4f_{7/2}$) was about 0.7eV at FWHM. During the XPS measurements, the specimen temperature was maintained at 295K (RT) or 160K (LT: low temperature). It was possible to irradiate the specimen surface with an external light generated by a tungsten lamp through Pyrex glass view port to enhance the surface photovoltaic effect.

6-3-3 Results and Discussions

Shown in Fig. 6-3-1 are a series of spectra of W(4f) and Ta(4f) regions taken at RT and LT with and without the external light source irradiated upon $TaSe_2$ = n-WSe_2 junction. A W(4f) spectrum from a freshly cleaved (0001) n-WSe_2 surface at RT is also shown for the binding energy reference. The estimated coverage of $TaSe_2$ was 6Å, equivalent to a monolayer. It is immediately identified that the W(4f) is shifted to the lower binding energy by 0.85eV at RT without external light source, indicating that band bending was induced by $TaSe_2$ deposition. When the external light was irradiated to the junction, the whole spectrum shifted toward the higher binding energy side by 0.42 eV without changing other features. This is due to the surface photovoltage induced by the external light. When the measurement was performed at LT without the external light, the observed binding energy shift for W($4f_{7/2}$) was much smaller than that measured at RT. Obviously the contribution of the photovoltaic effect induced by the incident x-ray becomes significant at LT. Applying the external light source to the specimen at LT, the binding energy for W($4f_{7/2}$) shifted further approaching to the original value of W($4f_{7/2}$) for the clean WSe_2 surface. Approaching to the flat band condition is strong evidence that the surface photovoltaic effect is saturated by the combined light irradiation of x-ray and external light sources. It indicates no Fermi level pinning takes place at the present interface.

An attempt to $TaSe_2$ / p-WSe_2 junction shows no surface photovoltaic effect as seen from the fact that no shift in the binding energy was observed for all conditions. This was expected since the work function for $TaSe_2$ is smaller than that for p-WSe_2, resulting the Ohmic behavior of the junction.

6-4. Conclusion and outlook

In this chapter, interfaces of layered semiconductors are studied in terms of chemical and electrical properties by using VDWE and XPS. It was found that $SnSe_2$ is epitaxially grown at the lowest substrate temperature (~230°C) ever achieved for VDWE of layered materials. The observed band bending was consistent with the work function difference between the film and the substrate, indicating the Schottky limit property of the junctions. As for the application of the films, low epitaxy temperature and high work function of $SnSe_2$ will be useful for the fabrication of organic/inorganic heterostructures and electric devices, respectively.

The photovoltaic effect at van der Waals interfaces was also studied. It was found that the value of photovoltage at low temperature is consistent with the amount of band bending. This "dynamic effect" at the interface will be useful to further investigate the electronic properties of the interfaces.

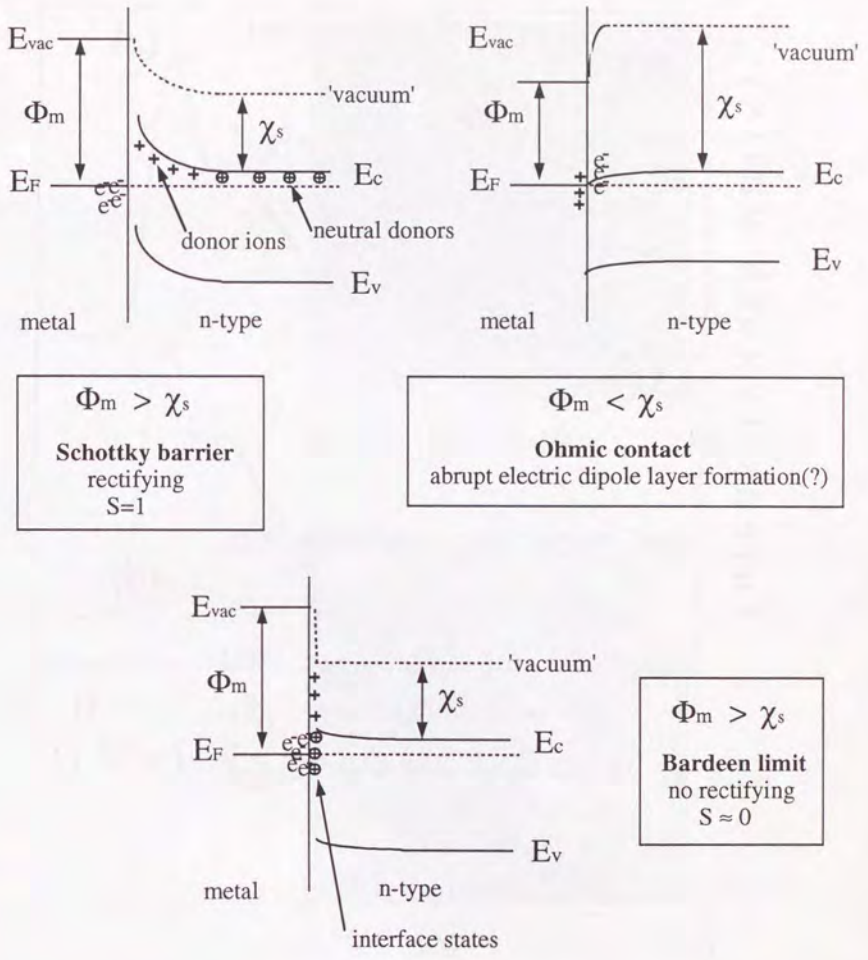

Fig. 6-1-1: Electronic properties and energy band alignment of metal-semiconductor interfaces (for n-type semiconductors). Φ_m and χ_s are work function of the metal and electron affinity of the semiconductor, respectively.

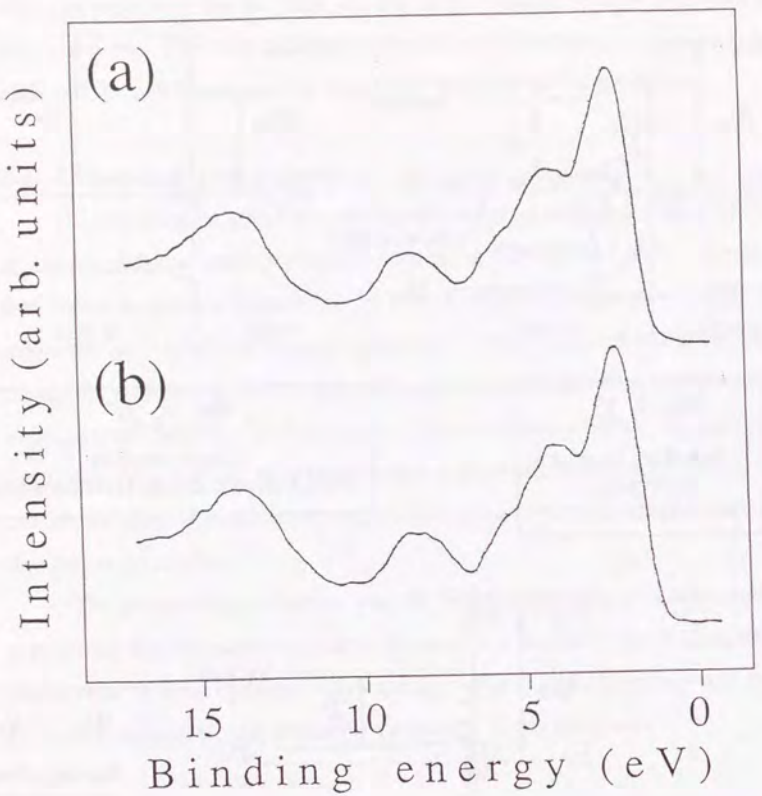

Fig. 6-2-1: XPS valence band spectra from (a) thick $SnSe_2$ film on MoS_2 and (b) bulk $SnSe_2$.

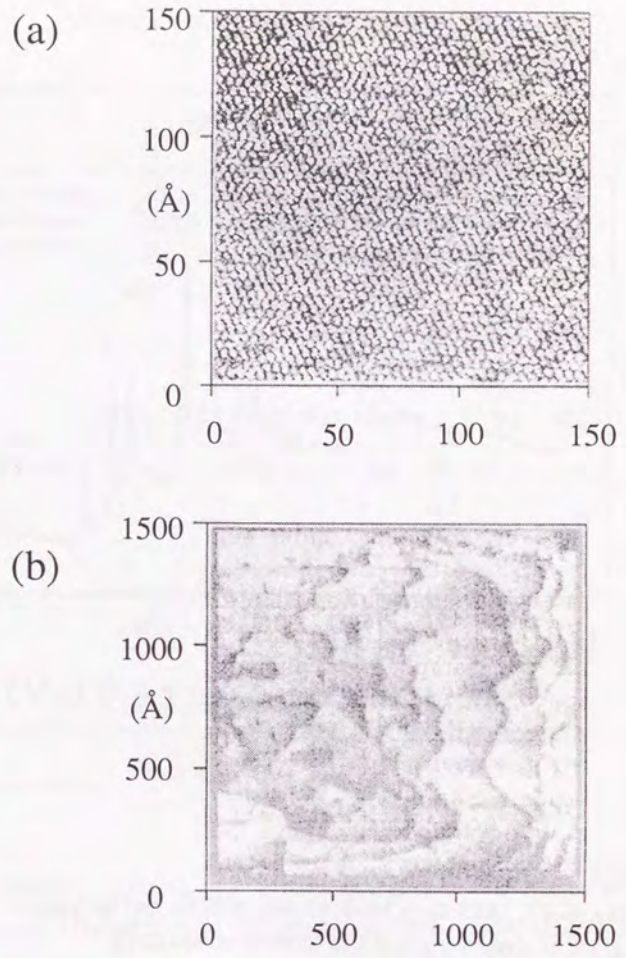

Fig. 6-2-2: STM images of $SnSe_2$ films.
(a) Atomic image of hexagonal lattice: lattice constant was consistent with that of $SnSe_2$. (b) Layered structure revealed by etching: height of the steps was consistent with that of $SnSe_2$.

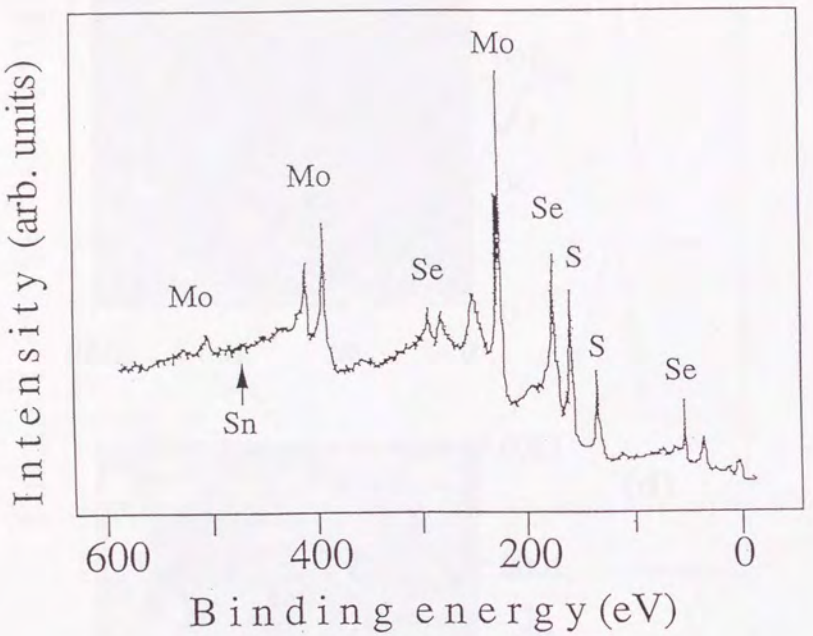

Fig. 6-2-3: XPS from MoS_2 treated with Sn and Se vapor at 550°C. Se signal is observed in addition to those of Mo and S.

Table 6-2-4. Core level shift of the elements in the heterojunctions compared to bulk materials.

M and X are components of substrate MX_2.

System	Shift (eV)			
	Sn	Se	M	X
$SnSe_2$ / $NbSe_2$	-0.55	-	0.00	-
$SnSe_2$ / MoS_2	0.00	0.00	-0.50	-0.50
$SnSe_2$ / HOPG	0.00	0.00	no shift (C(1s))	

Table 6-2-5 . Work functions .

Materials	$SnSe_2$	Film (on MoS_2)	$NbSe_2$	MoS_2	HOPG
Work function(eV)	5.3	5.3	5.9	4.8	4.5

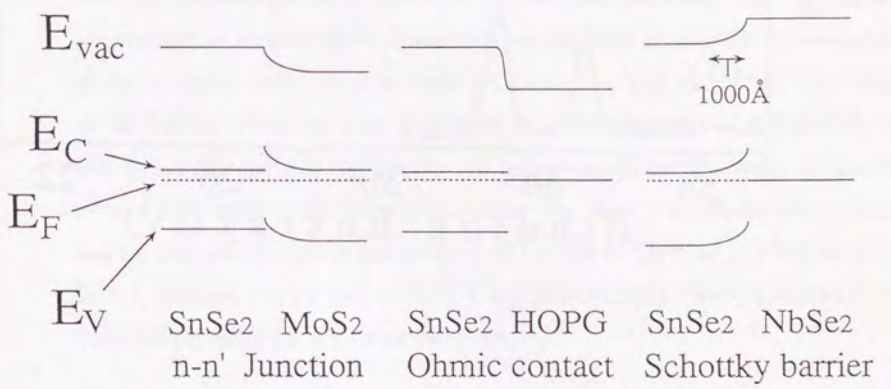

Fig. 6-2-6: Schematic diagram illustrating the electronic structures of $SnSe_2$ / layered material junctions.

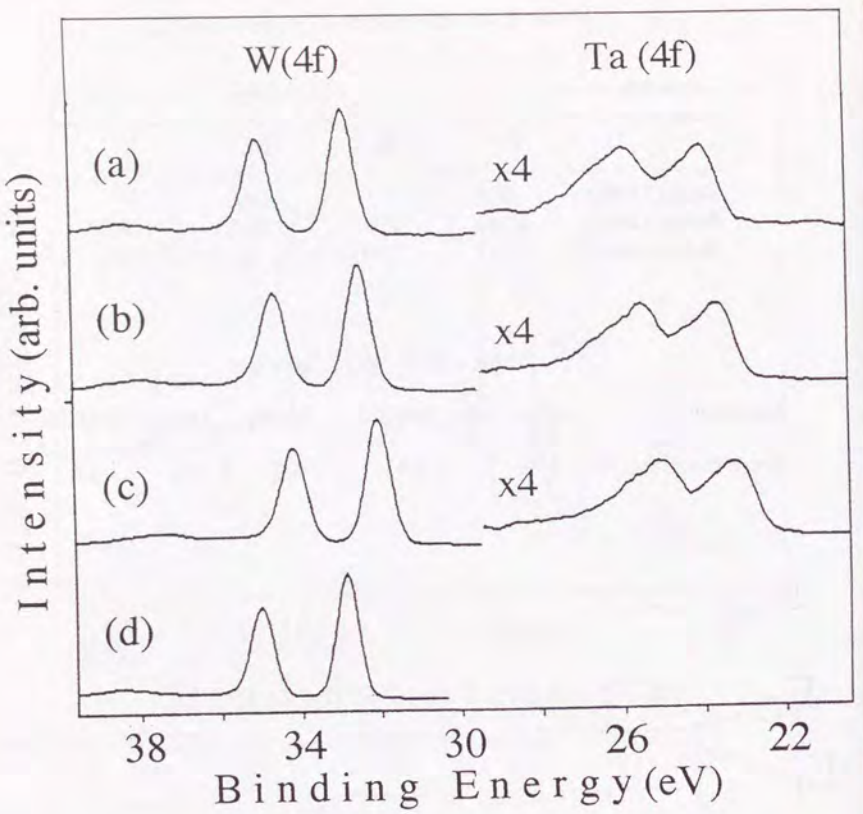

Fig. 6-3-1: XPS W(4f) and Ta(4f) core level spectra from a $TaSe_2$ monolayer / n-type WSe_2 junction. (a) illuminated at 160K, (b) illuminated at 295K, (c) dark at 295K, (d) bulk n-WSe_2. The band bending (core level shift of W(4f) between (c) and (d)) is 0.85 eV and the photovoltage ((core level shift of W(4f) between (c) and (a)) is 0.78 eV.

Chapter 7. Charge density waves at surfaces and interfaces of 1T-TaS_2

In this chapter, CDW of bulk 1T-TaS_2 at surfaces and interfaces is studied by the epitaxial growth of overlayers followed by the characterization using electron spectroscopies. In order to circumvent the thermal polytype transformation of 1T-TaS_2, a layered semiconductor $SnSe_2$ and metals with face centered cubic (FCC) structures were chosen as the overlayer materials. In section 7-1, VDWE of $SnSe_2$ on 1T-TaS_2 is reported. $SnSe_2$ is the only one among the layered materials which can be grown epitaxially on 1T- structure of TaS_2. CDW of underlying 1T-TaS_2 was not different from that of a bare surface. Next, the epitaxial growth of metals on 1T-TaS_2 was examined. Since the growth temperature of metallic layered materials are too high to maintain 1T- structure of the substrate, metal elements with FCC structure was attempted. The result of the surface chemistry after deposition is mainly reported in section 7-2. It was found that the Au, Ag, Cu, Pb can be grown epitaxially, while Ni and Al reacted with TaS_2 at the room temperature. Ag and Cu intercalated into TaS_2, and Cu changed the LEED pattern from $\sqrt{13} \times \sqrt{13}$ of CDW of 1T-TaS_2 to 3 x 3. In 7-3, electron energy loss (EELS), x-ray photoelectron (XPS) spectra of 1T-TaS_2 are provided for the future reference.

7-1. van der Waals epitaxy of $SnSe_2$ on 1T-TaS_2

7-1-1 Introduction

Charge density wave (CDW) has been the subject of interest in solid state physics [1]. While the CDW is induced by the instabilities caused by the nesting of Fermi surface in metals, its behavior at the surface and interfaces is not deduced *a priori*. In particular, the influences of CDW to overlayers and vice versa have not been studied so far. I therefore utilized VDWE to fabricate overlayers on 1T-TaS_2 which is known as a layered metal with noticeable CDW transitions. However, there was a problem with 1T-TaS_2. Its crystal structure (1T) is only meta-stable below ~800°C and it undergoes a polytype transformation when heated for long time above ~300°C, which restricts the selection of the grown materials. Since it was found that $SnSe_2$ can be grown at 230°C (section 6-2), VDWE of $SnSe_2$ and investigation of CDW using LEED and XPS are attempted in this section.

7-1-2 Experimental

VDWE of $SnSe_2$ was performed just as described in section 6-2. A single crystal of 1T-TaS_2 was cleaved in UHV with adhesive tape prior to the growth. After the growth, LEED and XPS were performed in the analysis chamber.

7-1-3 Results and discussions

A LEED pattern of 2ML $SnSe_2$ on 1T-TaS_2 is shown in Fig. 7-1-1, where the original ($\sqrt{13}$ x $\sqrt{13}$) pattern of TaS_2 is converted to (1x1) pattern of $SnSe_2$. LEED pattern did not show noticeable difference in the temperature range from 150K to 380K.

Peak positions of XPS core level spectra of Sn, Se and S in the $SnSe_2$ (1ML thickness) / 1T-TaS_2 system were identical with those of bulk $SnSe_2$ and 1T-TaS_2 when measured at 295K. It indicates no band bending took place at the interface, which is consistent to the coincidence of the work functions between TaS_2

(5.2eV) and $SnSe_2$ (5.3eV). Figure 7-1-2, -3 and -4 show the XPS Se(3d), S(2p) and Ta(4f) with Sn(4d) spectra at different temperatures. When the sample was cooled to 150K, Ta(4f) core level showed a splitting due to CDW exactly in the same manner as the bulk 1T-TaS_2 (Fig. 7-1-4). This result is explained by the fact that the amount of charge transfer is very small because of the coincidence of the work functions. The CDW in the underlying 1T-TaS_2 also indicates no reaction occurs at this VDWE-formed interface.

In Fig 7-1-2, it is noticed that Se(3d) shows narrowing of tails of the higher-biding energy side, while Sn(3d) spectrum did not change the peak shape observably. Since the change in the tailing of Se(3d) at different temperatures is not observed in $SnSe_2$ monolayer films grown on $NbSe_2$, it is probably the effect of underlying 1T-TaS_2. It was found that similar broadening occurs in the S(2p) core level XPS of 1T-TaS_2 (Fig.7-1-3). The tailing of S(2p) has been explained by [2] as the result of Mahan-Noziéries-DeDominicis (MND) effect [3] which is characteristic to metallic materials. It is a many body effect in XPS caused by the shielding of holes created by the photoemission process by free electron in the metals. As estimated from the electric conductivity of 1T-TaS_2, the number of conduction electron in 1T-TaS_2 decreases about 20 times during the nearly-commensurate to commensurate CDW transition. This is consistent with the observed decrease in the tailing of S (2p) and Se (3d) spectra. Therefore it is considered that the tailing is due to the MND effect. The MND effect in $SnSe_2$ must come from the electron tunneling from the surface of 1T-TaS_2 into $SnSe_2$ overlayer by the following two reasons. (i) $SnSe_2$ is a semiconductor and shows no MND effect by itself. (ii) The carrier transfer across the interface due to the band bending will not be temperature dependent because there is no change in the work function of the substrate 1T-TaS_2 associated with CDW (section 3-3). This explanation is supported by the fact the temperature dependence in the peak shape was only observed for Se atoms, which is facing the interface. From this consideration it is concluded that the tunneling from 1T-TaS_2 reaches to nearby

Se (~ 4.5 Å from Ta) but not to Sn (~ 6Å from Ta), assuming 3Å van der Waals gap between the film and the substrate. Theoretical consideration on MND effect, which is not available for the interfacial systems, is necessary for the further analysis. Since the estimation of the electron tunneling at the metal-semiconductor interfaces will be important for the pursuit of theoretically proposed 'excitonic' superconductivity which incorporates interfacial effects at metal-semiconductor interfaces [4].

7-2. Epitaxial growth, intercalation and reaction of metals with FCC crystal structures deposited on 1T-TaS_2 (0001) faces

7-2-1 Introduction

It is known that some of the metals with face centered cubic (FCC) structure form (111) hexagonal epitaxial lattices when deposited on (0001) surface of layered metal dichalcogenides (MX_2). Although sometimes reaction or intercalation with the substrates are observed depending upon the combination of the deposited metal and the substrate materials, there have been only a small number of studies on this system [5]. I have therefore started a systematic investigation on FCC-metal / 1T-TaS_2 interfaces.

The study of metal / 1T-TaS_2 interfaces has another importance for present investigation. The electric conductivity of TaS_2 and $TaSe_2$ epitaxial films has been measured as described in chapter 4. Since the electrode for the resistivity measurement necessarily consists of metal / TaS_2 or $TaSe_2$ interface, I focused the efforts on the interfaces of TaS_2. In this section, the deposition and chemical behavior of Au, Ag, Cu, Pb, Ni and Al on top of cleaved (0001) surfaces of 1T-TaS_2 under UHV condition is reported. XPS, LEED and STM were utilized for the analysis.

7-2-2 Experimental

Au, Ag, Cu, Ni and Al were evaporated from wire sources hanging from Joule-heated W-coil in UHV. Pb source was a crucible source made of Mo which was heated by electric current. The sources were situated in a small chamber connected with the analysis chamber. The opening of the crucible source was directed toward the specimen, while metals from the wire sources were emitted to all direction. The chamber was pumped with an ion pump during the degassing of the source by preheating. After the cleaning of the metal source, the gate valve between the source chamber and the analysis chamber was opened, and the metal was deposited on the sample surface. The 1T-TaS_2 specimen was cleaved in UHV with Cu adhesive tapes and transferred to the analysis chamber. After the deposition, sample surfaces were investigated with XPS and LEED. The sample temperature was monitored with a K-type thermocouple and was maintained at room temperature throughout the experiment unless mentioned otherwise.

7-2-3 Result and discussion

A. Ag

After sub-monolayer amount of Ag was deposited, $\sqrt{13} \times \sqrt{13}$ structure of TaS_2 was maintained. However, the intensity of the Ag(3p) photoelectron decreased in the scale of hours after the deposition (Fig. 7-2-1). It indicates the intercalation of Ag into 1T-TaS_2. When a large amount of Ag is deposited, LEED pattern became 1 x 1 of Ag(111).

B. Cu

Just with a sub-monolayer amount of Cu deposited, LEED pattern changed from $\sqrt{13} \times \sqrt{13}$ to 3 x 3. Cu (2p) peaks in XPS decreased in the time scale of seconds, which indicates rapid intercalation of Cu into 1T-TaS_2 (Fig. 7-2-1). LEED pattern of the lower spectrum in Fig. 7-2-1 was diffuse $\sqrt{13} \times \sqrt{13}$, which indicates CDW of the top surface is resumed after Cu have diffused in the lower layers. When a large amount was deposited, 1 x 1 LEED pattern of Cu(111)

appeared, but it decayed eventually and the pattern recovered 3 x 3 and then to $\sqrt{13} \times \sqrt{13}$.

Chemical state of Cu was studied from characteristic peak shape of XPS Cu(2p) and Cu L_3VV Auger emission (Fig. 7-2-2). Since the XPS spectrum does not show the satellite peaks which is characteristic to Cu^{2+}, the chemical state is Cu^{1+} or Cu^0. From observed shift in AES it was concluded that the intercalated Cu is Cu^{1+}. Figure 7-2-3 shows XPS Ta(4f) of Cu- intercalated 1T-TaS_2 and genuine 1T-TaS_2 substrate with that of H_2- intercalated 1T-TaS_2 for reference [6]. The peak shape of Cu / 1T-TaS_2 is different from that of genuine 1T-TaS_2 considerably, which suggests 3 x 3 LEED pattern is caused by the modification of CDW. The peak shape was identical to that of H_2- intercalated 1T-TaS_2 [6]. Since it is established from NMR measurement that hydrogen is intercalated to 1:3 atomic ratio with Ta (i.e. $H_{0.33}TaS_2$) [7], present result probably indicates that the atomic ratio of Cu is also 1:3 to Ta and that this peak shape is characteristic to the to 1T-TaS_2 with an electron donated per three Ta atom.

The intercalation of Cu has been published independently by Pettenkofer et al [8] and the chemical state of Cu was determined by the same method.

C. Ni

Deposition of Ni results in a very diffuse 1 x 1 LEED pattern. As seen from Figure 7-2-4 showing S(2p) peak shape after the deposition of Ni, a reaction between Ni and the substrate 1T-TaS_2 occurs upon deposition. A halo LEED pattern was observed after a large amount of Ni was deposited.

D. Au

Au did not intercalate into 1T-TaS_2 within the time scale of 24 hours, nor changed CDW of 1T-TaS_2. However, when the sample temperature became higher (but less than ~100°C) during the deposition, S(2p) XPS showed a broadening just as in the case of Ni, which suggests a reaction. Further study on the temperature dependence of Ta(4f) core level XPS of Au / 1T-TaS_2 was desired in order to unveil the microscopic nature of image forces in the metals

which cannot be treated in the band calculation at present. However, there was a problem. Figure 7-2-5 is a STM image showing the morphology of Au epitaxial film on 1T-TaS_2. Island structure of Au film is clearly observed. In order to study the overlayer effect of CDW by electron spectroscopy, the substrate 1T-TaS_2 must be covered completely and 'seen through' the overlayer. This condition can probably satisfied even for the island morphology, after a large amount is deposited. However, much larger amount of the deposit than $SnSe_2$ is needed and the signal from the covered substrate is very weak. This problem could not be solved in the present study. Since this overlayer effect of CDW will be important in the development of the fundamental theory of solid state physics, this interface should be revisited in the future with the photoemission using strong synchrotron radiation.

E. Other metals

The results including other FCC-metals are summarized in the Table below.

Table: Metal deposition on 1T-TaS_2.

	Reaction	Intercalation	Epitaxy	LEED	ionic state
Au	-	-	O	$\sqrt{13}x\sqrt{13}$	0
Ag	-	+	O	$\sqrt{13}x\sqrt{13}$	?
Cu	-	++	O	3x3	1+
Ni	++	+	X	1x1	?
Al	+	-	O	1x1?	?
Pb	-	-	O	$\sqrt{13}x\sqrt{13}$	?

(++: observed in less than 1~10 min; +: observed in 24h; -: not observed in 24h; O: epitaxy; X: no epitaxy)

Now let us discuss the application of these metals for electrodes in electronic property measurement. It is desired that the electrode forms a mechanically strong, low resistivity Ohmic contact with the substrate without

changing the physical property of the specimen. Since the metals other than Au and Pb intercalate or react with the substrate, it follows that Au or Pb is suitable for the electrode material deposited on the TaS_2 specimens. Considering Pb is reactive with water or oxygen, Au is concluded as the best choice. It should be noted that Cu must be avoided in the contact with TaS_2 because it intercalates rapidly (in the time scale of seconds) and changes CDW of the material.

7-3. Electron spectroscopy of 1T-TaS_2

Surfaces of 1T-TaS_2 is the subject of interest since the discovery of its CDW. Various surface characterization methods have been applied, including XPS [2], UPS [9], and recent application of STM [10] and electrochemical STM [11]. However, the published spectra are limited. In this section, spectroscopic data of 1T-TaS_2 measured in the present research are shown for the future reference. Figures 7-3-1 and -2 are EELS spectra, and Fig. 7-3-3 shows XPS valence band spectra of different CDW states of 1T-TaS_2.

7-4. Conclusion and outlook

VDWE of $SnSe_2$ on 1T-TaS_2 (0001) did not affect the CDW of the substrates. On the other hand, XPS of $SnSe_2$ showed temperature dependent MND effect which is only observed in metals. It indicates the conduction electrons tunnel into the $SnSe_2$ overlayer.

Some metals with FCC crystal structure (Au, Ag, Cu, Ni, Al, Pb) was deposited onto (0001) faces of 1T-TaS_2 and the possibilities of epitaxial growth, intercalation and reaction were investigated with XPS and LEED. It was found that Au and Pb did not react or intercalate with 1T-TaS_2 at room temperature, showing good applicability for the electrode for the measurement of electronic properties of TaS_2 films. Although both of Cu and Ag intercalated into 1T-TaS_2, their effects on CDW of the substrate were different. Cu-TaS_2 changed CDW to 3 x 3 but Ag-TaS_2 maintained $\sqrt{13}x\sqrt{13}$ LEED pattern. It is probably due to the

electron numbers donated per intercalated atoms are different. Further study on this system, especially temperature dependence of Ta(4f) core level XPS of Au / 1T-TaS_2 is desired in order to unveil the microscopic nature of image forces in the metals which cannot be treated in the band calculation at present. The use of synchrotron radiation will be promising for the measurement of the photoemission from Au covered 1T-TaS_2.

Fig. 7-1-1: A LEED pattern of $SnSe_2$ (2ML thickness) / 1T-TaS_2. Accelaration voltage is 115eV.

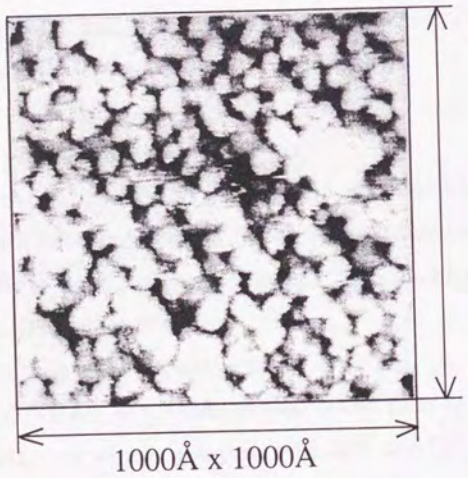

Fig. 7-2-5: An STM image showing the morphology of an Au epitaxial film grown on 1T-TaS_2 at room temperature.

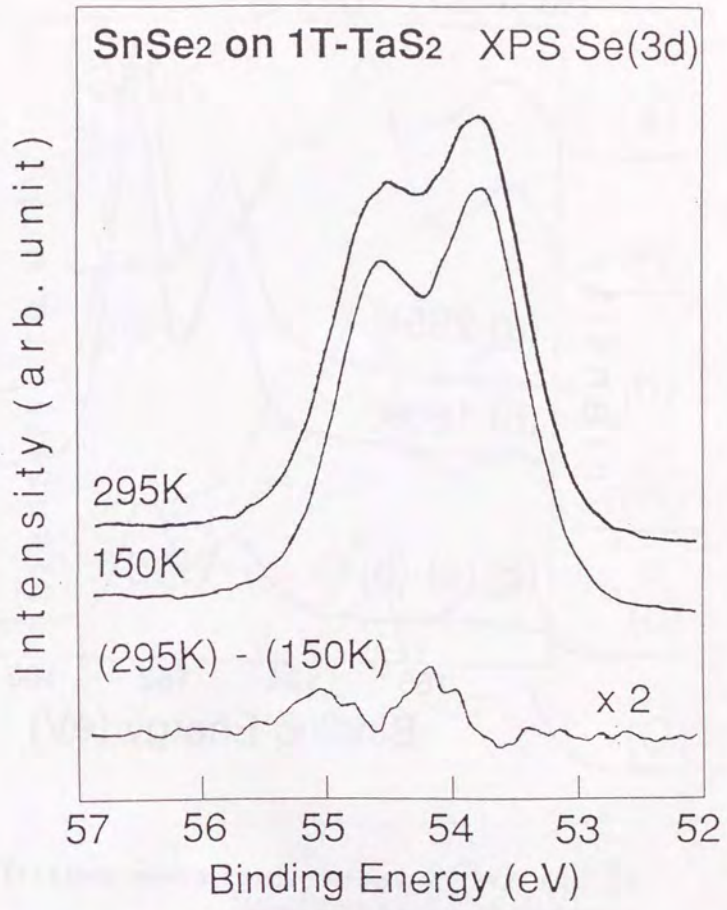

Fig. 7-1-2: XPS Se(3d) core level spectra of $SnSe_2$ (2ML) / 1T-TaS_2 taken at 295K and 150K, and their diffrence.

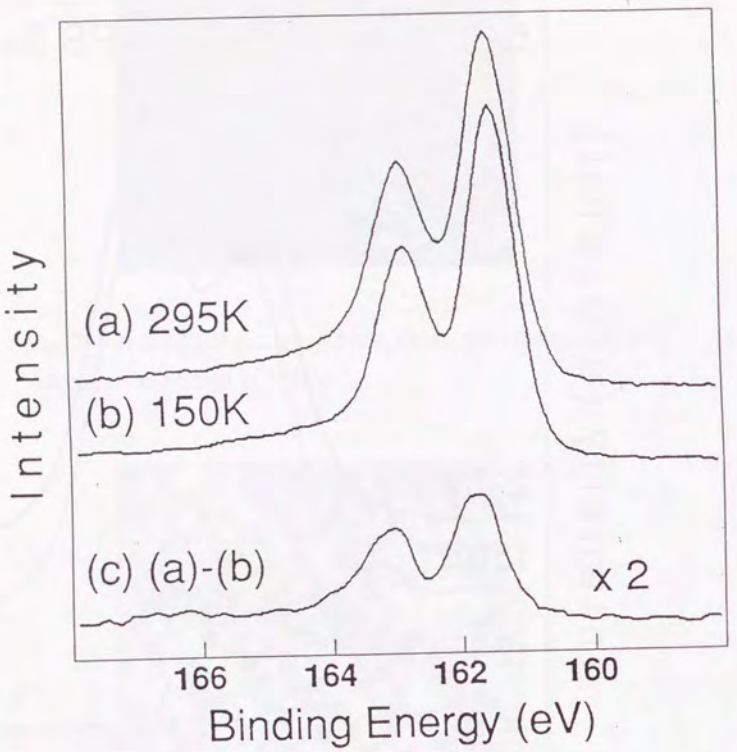

Fig. 7-1-3: XPS S(2p) core level spectra of $SnSe_2$ (2ML) / 1T-TaS_2 taken at 295K and 150K, and their diffrence.

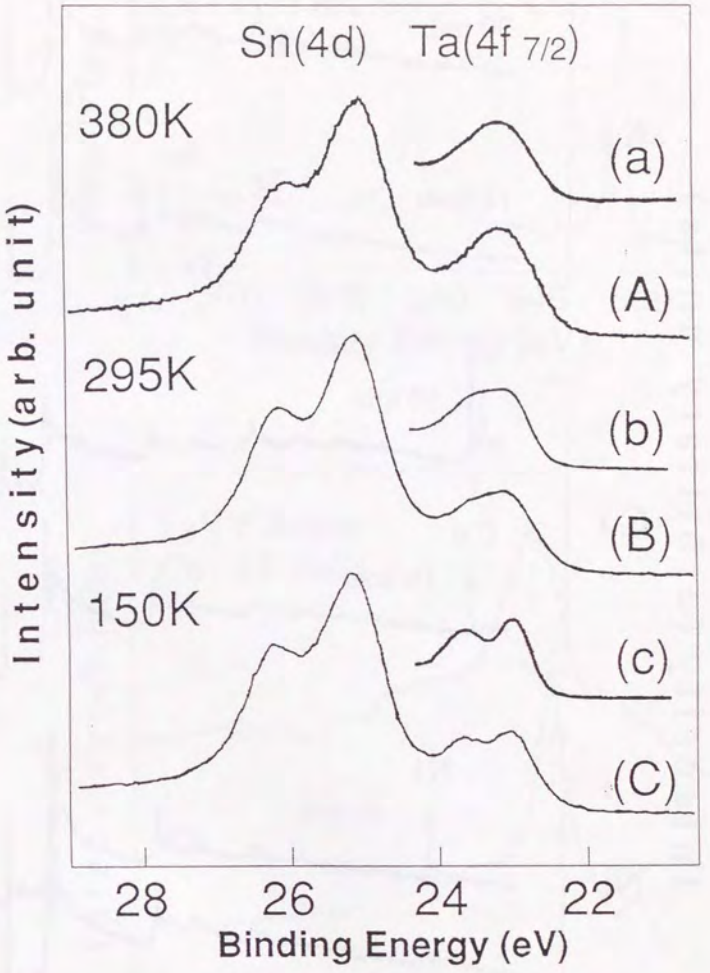

Fig. 7-1-4: (A) (B) (C): XPS Ta($4f_{7/2}$) and Sn(4d) core level spectra of $SnSe_2$ (2ML) / 1T-TaS_2 taken at various temperatures. (a) (b) (c): XPS Ta($4f_{7/2}$) core level spectra of bulk 1T-TaS_2 taken at the same temperatures with (A)-(C).

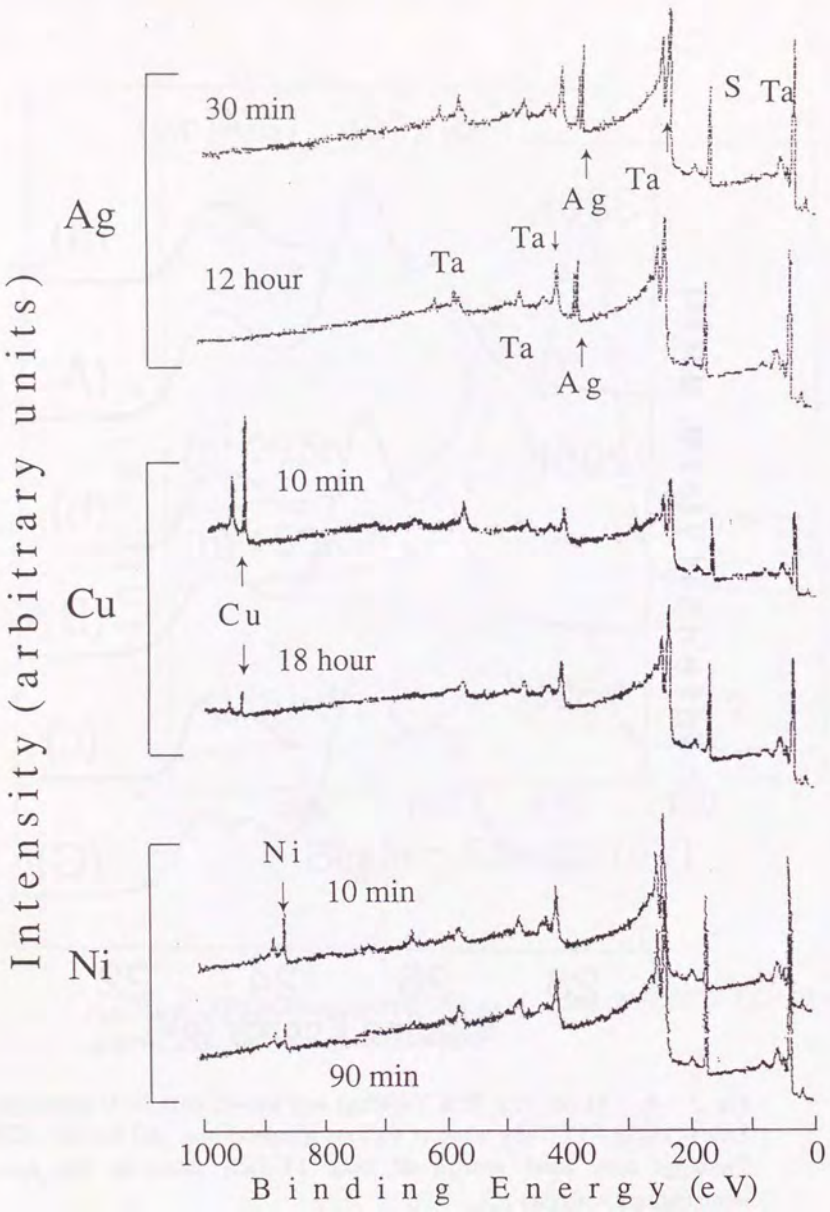

Fig. 7-2-1: Time dependence of XPS (Al Kα) spectra of metal (Ag, Cu, Ni)- deposited 1T-TaS_2. The time in the figure is the interval between the deposition and the measurement.

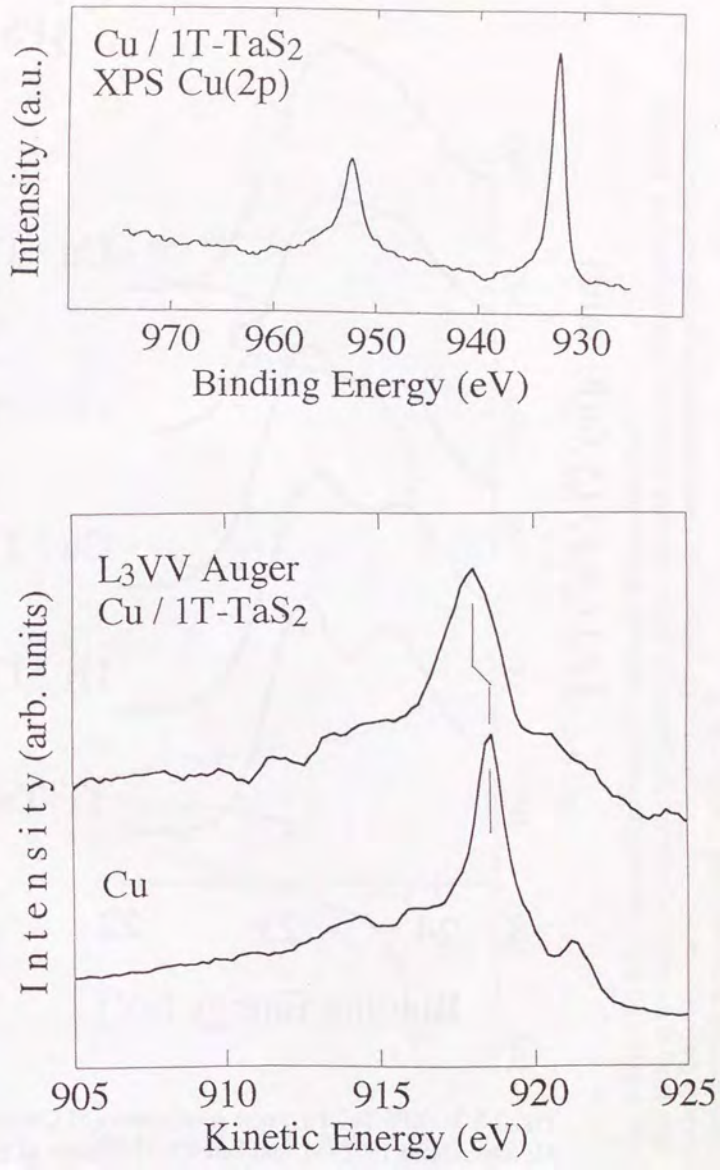

Fig. 7-2-2: XPS Cu(2p) core level spectrum and Cu L_3VV Auger spectrum from Cu-intercalated 1T-TaS_2 and Ar^+ spatter-cleaned Cu foil. It can be seen that the ionic state of intercalated Cu is Cu^{1+}.

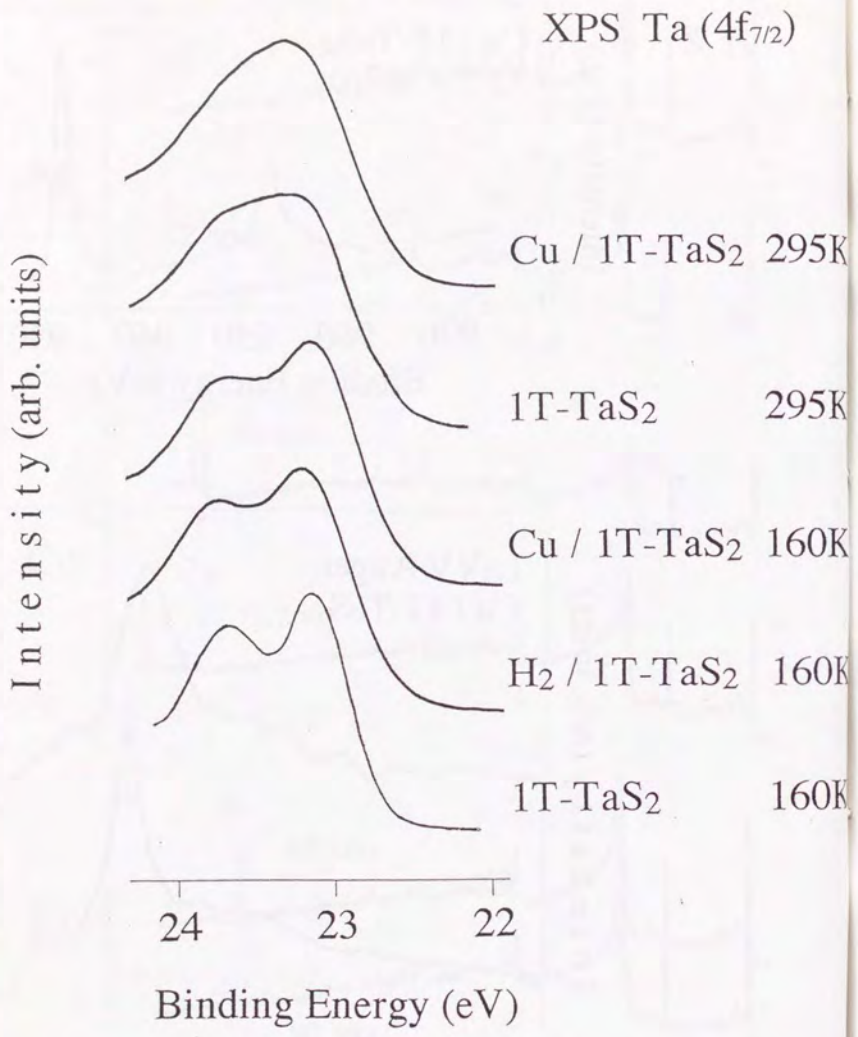

Fig. 7-2-3: XPS Ta($4f_{7/2}$) core level spectra of Cu-intercalated 1T-TaS_2, H_2-intercalated 1T-TaS_2, and bulk 1T-TaS_2 taken at 295K and 160K.

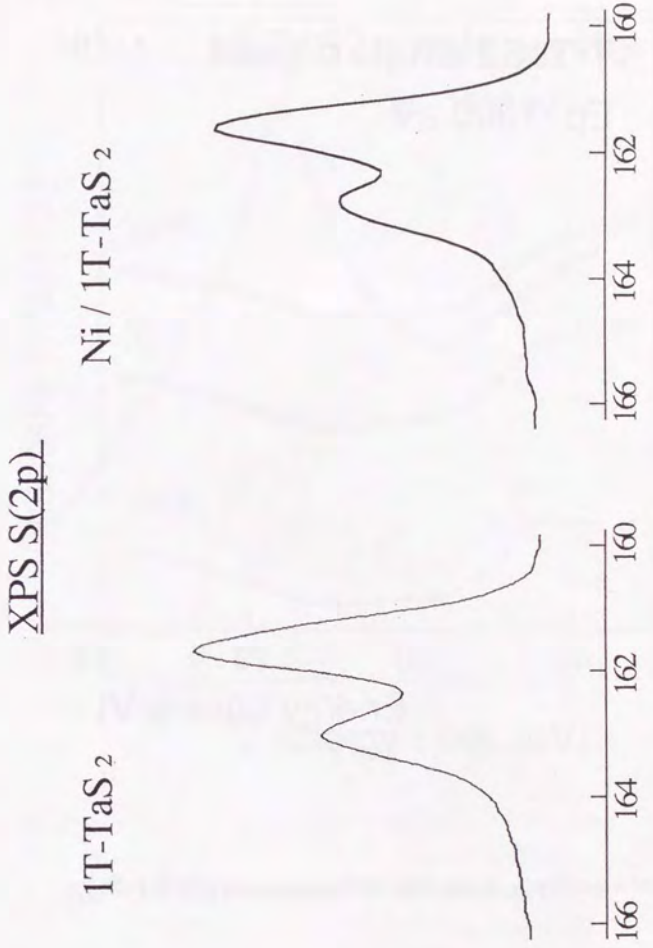

Fig. 7-2-4: XPS S(2p) spectra from clean 1T-TaS2 and Ni deposited TaS2.
The depth of the valley between the two peaks splitted by spin-orbit interaction is shallower in Ni deposited sample than clean surface. It is interpreted as the evidence for other chemical component with different chemical shift produced by the reaction with Ni.

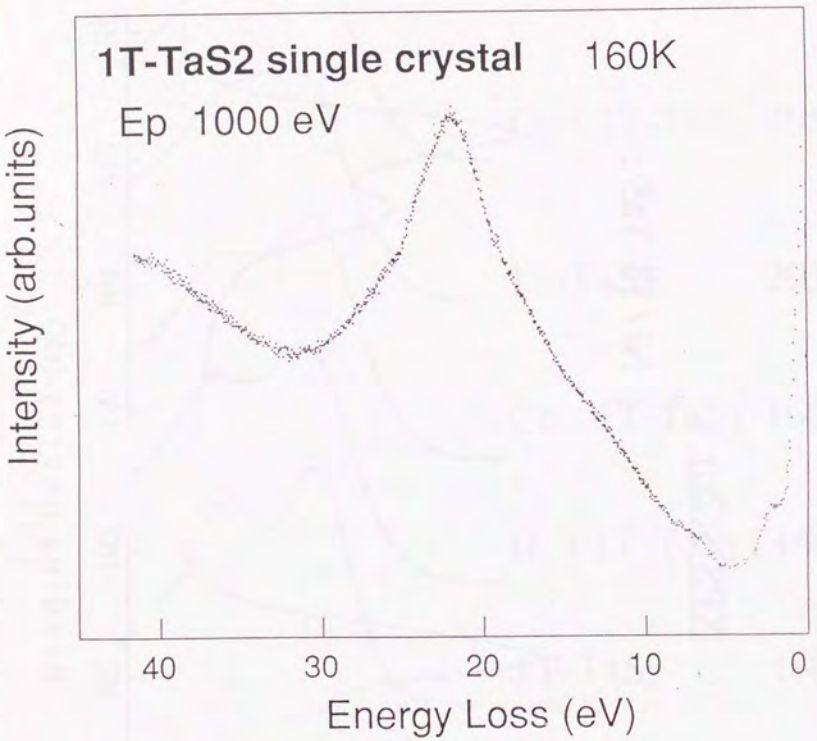

Fig. 7-3-1: An EELS spectrum of 1T-TaS_2.

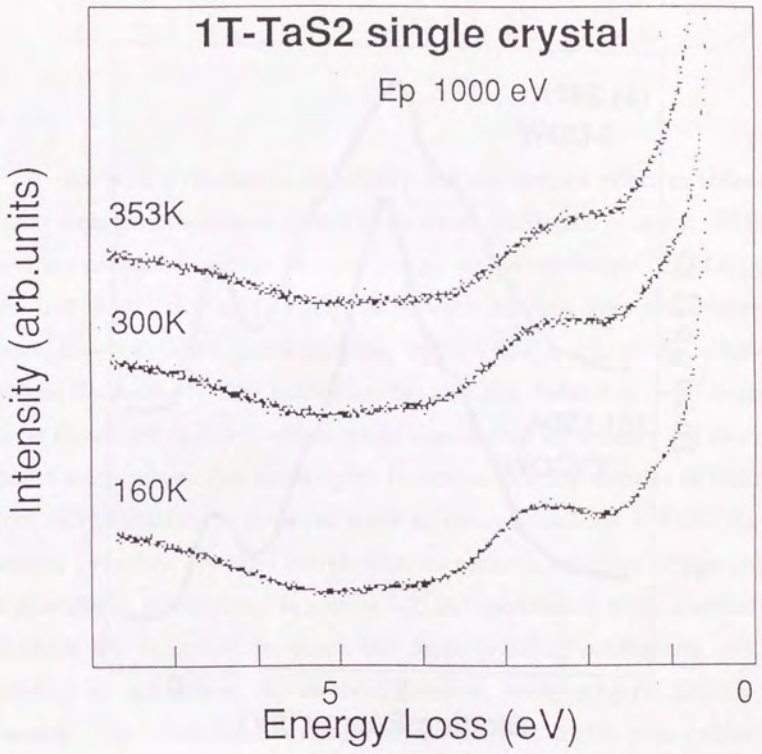

Fig. 7-3-2: EELS spectra of 1T-TaS_2 taken at different temperatures.

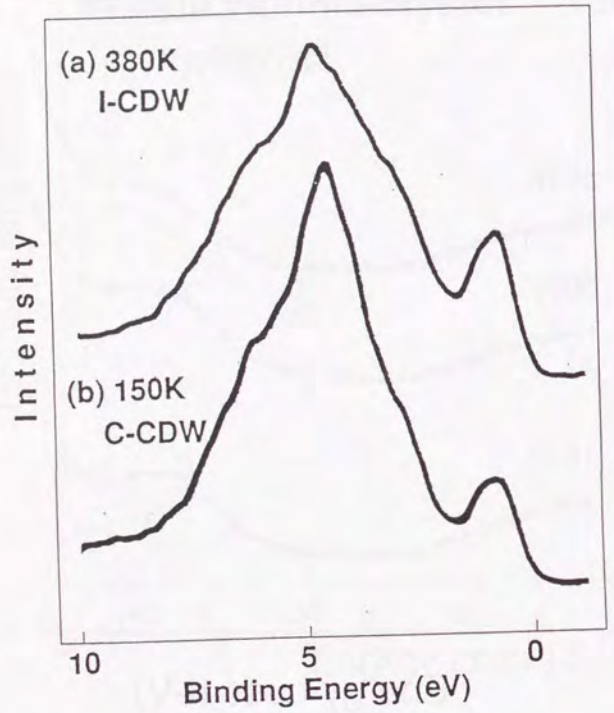

Fig. 7-3-3: XPS valence band spectra of 1T-TaS_2 taken at different temperatures. Al Kα x-ray was used.

Chapter 8. Interference effects in reflection electron energy loss spectroscopy

In this section, excitation probability and interference effect in reflection electron energy loss spectroscopy (REELS) are studied experimentally. REELS, sometimes called low energy electron energy loss spectroscopy (LEELS), is a useful tool in the study of the interfaces between ultrathin films and substrates, because non-destructive depth-profiling up to a few nm is easily achieved. However, the depth-profiling mechanism has not been clarified in detail so far. I became interested in this problem while considering an analogy for recently invented electron emission holography. In section 8-1, the theories of electron energy loss probability is reviewed since no concise textbook is found on the reflection geometry. A brief introduction on electron emission holography is also provided in this section. In section 8-2, an experimental study and analysis of REELS are described, in which the depth profiling mechanism and the possibility of performing the electron emission holography in REELS are discussed. The experiments were performed using a double-pass cylindrical mirror analyzer (CMA) for cleaved surfaces of $MoSe_2$ and epitaxial films of Ag grown on MoS_2.

8-1. Theoretical review of reflection electron energy loss spectroscopy (REELS)

8-1-1 Processes involved in REELS

In the measurement of REELS, electrons of a certain incident energy (Ep) is introduced to the sample surface and nearly back-scattered electrons are collected by an electron energy analyzer. Since the electrons must be back-scattered in REELS, successive diffraction is strongly involved [1]. The important processes are "back-scattering loss" (L), "forward-scattering loss before back-scattering diffraction" (LD) and "back-scattering diffraction before forward-scattering loss" (DL) as illustrated in Fig. 8-1-1. There are two processes of the energy loss as follows.

(i) Bulk loss: Electrons lose their energy by the interaction of the elementary excitation inside the solid.

(ii) Surface loss: Electrons interacts with the dipole electric field extended from the surface which is created by the density wave of the surface charges associated with the excitation in the vicinity of the surface.

The elementary excitations include electron excitation and phonon excitations. Among the electron excitations, plasmons, interband transitions and core level electron excitations are observed strongly in REELS. Surface loss is usually only observable for plasmons among the electron excitations.

8-1-2 Energy loss function

It is widely accepted that the electron energy loss probabilities in the bulk and at the surface are proportional to so called energy loss function $\mathrm{Im}(- \varepsilon(\omega,q)^{-1})$, and surface loss function $\mathrm{Im}(- (\varepsilon(\omega,q)+1)^{-1})$, where $\varepsilon(\omega,q)$ is the dielectric constant, ω and q are the angular frequency and the momentum of the excitation [2]. However, they are not sufficient for the analysis of E_p-dependence of the loss probability because factors dependent on q is multiplied as is shown in the following.

The energy loss probability of the bulk loss is given by several authors using semi-classical (Ohm's law) [3] or quantum mechanical [4] consideration, both of which give:

$$\partial^3 W_b/\partial\Delta E\partial^2\Omega \propto q^{-2}\,\mathrm{Im}(-\varepsilon^{-1}), \qquad (8\text{-}1\text{-}1)$$

where Ω is the solid angle in the direction of the exiting electron, and ε is the dielectric constant of the sample. q is the momentum of the excitation.

As for the surface loss measured with the incident electrons normal to the surface, the differential cross section is [5]

$$\partial^3 W_s/\partial\Delta E\partial^2\Omega \propto [4R_{LD}R_{DL}\,q_s\,q^{-4} + (R_{LD} - R_{DL})\,q_s^{-1}q^{-2}] \times \mathrm{Im}(-(\varepsilon+1)^{-1}), \qquad (8\text{-}1\text{-}2)$$

where q_s is the component of q parallel to the surface, R_{LD} and R_{DL} are the elastic reflection probability for the LD and DL processes, respectively. It must be noted that Born approximation which is only valid for the high E_p (>1000eV) is used in the above calculations.

Now let us calculate the excitation probability for the comparison with the experimental results. First the plasmons are treated. The L process is forbidden for the plasmons measured in the reflection geometry with $E_p > 10$eV because there is a cut-off wave number where the plasmon collapse into electron-hole pairs. For the bulk plasmons with ω near the plasma frequency at which we are doing the measurement, $\mathrm{Im}(-\varepsilon(\omega,q)^{-1})$ can be written as [4]

$$\mathrm{Im}(-\varepsilon(\omega,q)^{-1}) = (\omega_q / 2)\,\delta(\omega-\omega_q)\,, \qquad (8\text{–}1\text{–}3)$$

where $\omega_q = \omega_p\,[1+ (3/10)\,q^2v_F / \omega_p^2 + ...] \approx \omega_p$ is the q-dependent frequency of the plasmon, $\omega_p = \Delta E/\hbar$ is the plasma frequency for q=0 , and v_F is the Fermi velocity. By integrating eq. (8-1-1) over q and over ω in the vicinity of the plasmon excitation ($\omega\approx\omega_p$) after replacing $\mathrm{Im}\,(-\varepsilon(\omega,q)^{-1})$ with eq. (8-1-3) , we obtain

$$W_b \propto \sqrt{\frac{E_p - \Delta E}{E_p^{\,3}}} \cdot \log\left(\frac{q_c}{k-k'}\right), \qquad (8\text{-}1\text{-}4)$$

where $k = \frac{\sqrt{2meE_p}}{\hbar}$, and $k' = \frac{\sqrt{2me(E_p - \Delta E)}}{\hbar}$.

In the above, the integration range was restricted by a minimum and maximum momentum transfer (q_{min} and q_{max}, respectively). $q_{min} = k - k'$ is given by the energy conservation while $q_{max} = q_c$ is determined by the plasmon cut-off.

As for the surface plasmons measured with the incident electrons normal to the surface, the integration of eq. (8-1-2) gives the cross section per unit time:

$$W_S \propto 4R_{LD}R_{DL}\,[I_S(q_c) - I_S(k-k')] + (R_{LD} - R_{DL})\,[J_S(q_c) - J_S(k-k')], \qquad (8\text{-}1\text{-}5)$$

where

$$I_s(q) = \frac{\sqrt{-q^4 + 2(k^2 + k'^2)q^2 - (k^2 - k'^2)^2}}{q^2} + \arcsin\left(\frac{-q^2 + k^2 + k'^2}{2kk'}\right) + \frac{k^2 + k'^2}{k^2 - k'^2} \cdot \arcsin\left(\frac{(k^2 + k'^2)q^2 - (k^2 - k'^2)^2}{2kk'q^2}\right)$$

$$J_s(q) = \frac{k'}{k^2 - k'^2} \cdot \arctan\left(\frac{k + k'}{k - k'} \tan\sqrt{\frac{q_c^2 - (k - k')^2}{(k + k')^2 - q_c^2}}\right).$$

The cross section for the core level excitation per incident electron averaging the momentum transfer is given semi-empirically by using atomic approximation as [6]:

$$W_C \propto (U\text{-}1)U^{-2} \ln(1.25U) \qquad (8\text{-}1\text{-}6).$$

Here $U = E_p / \Delta E$, where E_p and ΔE are the energy of the incident electron and the loss energy, respectively.

By ending this subsection, it should be noted that the duration of interaction is not included in the above expressions. It is related with the probing depth of REELS, which is not fully understood for low E_p. Estimation of it as a function of E_p from the experimental results is also attempted in the following.

8-1-3 Electron emission holography and REELS

Recently, holographic interpretation of interference patterns in angle resolved photoemission (PES) and Auger electron spectroscopy (AES) draws a wide attention in the surface science community [7]. Although the possibility of similar analysis for electron energy loss spectroscopy (EELS) was suggested at the early stage of the researches [8], there have been no reports on investigations about this matter, at least in terms of experiments, to the authors' knowledge. Holographic interpretation of angle resolved PES or AES data utilizes the fact that the electron of the measured energy is emitted from certain atomic species which can be regarded as point sources. Then these electrons are scattered by surrounding atoms and make interference patterns which can be analyzed as a modified holography [7]. Although there are two types of measurement geometry in EELS, i.e., transmission and reflection EELS, the possible analogue of the electron holography will be the reflection type. In particular, core level excitations might be treated as point sources. However, there is a major difference between core level REELS and ordinary electron-emission holography. Since the electrons must be back-scattered in REELS, successive diffraction is strongly involved in the observed intensity as mentioned in section 8-1-2. In the following section, the experimental assessment of the "electron energy loss holography" is also considered.

8-2. Experimental study on incident energy dependence of REELS intensity

8-2-1 Introduction

As reviewed in the previous section, the excitation probabilities can be obtained theoretically. However, there are several important points not revealed at present. (i) The theories have not been confirmed experimentally, especially for low E_p's which are utilized in REELS. (ii) The duration of interaction, which is important in the depth profiling analysis of REELS, is not known. (iii) The removal of the loss process involving diffraction might lead to an analogue

of electron emission holography in REELS, but it has not been studied. With those backgrounds, I measured the Ep-dependence of the REELS intensity of various electron excitations with a double-pass CMA. The samples were (0001) surfaces of a layered semiconductor $MoSe_2$ and epitaxial films of Ag with (111) faces. $MoSe_2$ was desirable for our purpose because it has no surface states [9] which would complicate the analysis, while Ag was chosen as a typical metal with inert surfaces. The measured excitations were bulk valence plasmons in $MoSe_2$ and Ag, core excitations of Se(3d) and π-plasmon in $MoSe_2$, and free electron plasmon of Ag.

8-2-2 Experimental

EELS was measured with a double pass CMA (PHI 15-255G) in the retarding mode without angle resolution. The CMA was placed at the angle normal to the specimen surface. The incident electrons were introduced along the axes of the cylinder. Besides the intensity of inelastic scattering, that of the elastic scattering was measured for the normalization. E_p was changed from 50 eV to 500 eV, although the identification of the loss peaks become difficult at lower E_p because of the strong secondary electrons.

A specimen of $MoSe_2$ was cleaved just before loading into the ultrahigh vacuum (UHV) chamber. The samples was heated in the UHV chamber at 200°C to remove small amount of contamination. The cleanliness and the crystallinity of the surface were confirmed by AES and reflection high energy electron diffraction (RHEED), respectively. Epitaxial films of Ag were prepared on MoS_2 (0001) faces by deposition of thermally evaporated Ag at room temperature in UHV. RHEED patterns indicated that Ag(111) surfaces were formed epitaxially. The growth of the Ag films was continued more than 10 times longer after the signal of the substrate MoS_2 was extinguished in RHEED and AES. The thickness of the film was estimated to be at least 300Å, which ensures that the effect of the substrate to EELS was negligible. The EELS

measurement was performed under the vacuum of $3x10^{-8}$ Pa. No contamination of the sample surfaces was detected by AES after the measurement.

8-2-3 Results

A. $MoSe_2$

Figure 8-2-1(a) shows an energy loss spectrum of $MoSe_2$ at E_p=300eV. Three peaks at 8.5 eV, 24 eV and 55 eV are identified as π-plasmon, bulk plasmon and Se(3d) core level excitation, respectively. Figure 8-2-2 shows the intensity of elastic scattering as a function of E_p, which is similar to I-V (intensity-voltage) curve in low energy electron diffraction (LEED). Several well defined peaks are easily recognized. The shape of the envelope function in the I-V curve changed when the distance between the sample and the CMA was altered, whereas the peak positions were maintained. This is probably caused by the focusing condition of the electron optics. In order to eliminate this effect and correct the difference in the intensity of the primary electron versus E_p, the inelastic intensities were normalized with the elastic. The inelastic intensities were obtained by integrating the area of the peaks after the subtraction of the backgrounds. The background was approximated by a line which passes the minima before and after the peak. The ratio after the normalization did not change noticeably with the sample position. The normalized intensities of π-plasmon, bulk-plasmon and Se(3d) core excitations are shown in Fig. 8-2-3.

B. Epitaxial films of Ag

A loss spectrum of a Ag film at 300 eV is shown in Fig. 8-2-1(b). Two distinctive peaks corresponding to free-electron plasmon (3.4eV) and bulk-valence-plasmon (17eV) were observed, while a weak shoulder of surface-valence-plasmon(11eV) is noticeable. The I-V curve for the Ag film was basically featureless, which was different from $MoSe_2$. The loss intensities normalized by the elastic peaks are shown in Fig. 8-2-4 by dots.

8-2-4 Discussions

The elastic I-V curve in Fig. 8-2-2 exhibits a strongly oscillating structure. When the abscissa of the graph is transformed to $\sqrt{Ep}$, the period of the oscillation becomes nearly a constant. It indicates that the wavenumber of the electron, which is proportional to $\sqrt{Ep}$, is a good parameter for the oscillation. It means that the oscillation is due to diffraction. The corresponding length in the real space is estimated to be 6Å~7Å. This length is in good agreement with the distance of unit layers in $MoSe_2$ (6.455Å [10]). The indexes of reciprocal lattice perpendicular to the layer are written in Fig. 8-2-2 for the peak position. I could not observe the diffraction caused by the atomic arrangement within a layer in $MoSe_2$, nor any oscillating feature in Ag. It is probably because CMA did not have the steep selectivity for the polar angle, although it is often mentioned that CMA only collects electrons with 42.3° polar angle. The reason is considered to be partly the non-zero pass energy of CMA and partly the ill-focusing caused by the E_p-dependence of the focusing position. Probably the effect of atomic arrangement other than the outstanding slab structure of $MoSe_2$ is smeared out by the angle integration of CMA. In the following we assume the diffraction parallel to the surface can be neglected.

Since the ratio of the inelastic to the elastic intensity was almost unchanged by moving the sample position, it seems that our normalization procedure was approvable. In order to separate the processes shown in Fig. 8-1-1, one can utilize the result of inelastic LEED [11]. When E_p is varied, each Bragg condition for diffraction will be satisfied twice corresponding to DL and LD. While the diffraction peaks in DL process are characterized with E_p, those in LD is determined with $E_p - \Delta E$. Accordingly, after the normalization by the elastic I-V curve, the intensity of LD will be much smaller than that of DL at the peak position of the elastic intensity. This assumption can be examined by comparing the experimental results with the theoretical calculation. The inelastic intensity after normalization will be roughly proportional to the loss probability, because

diffraction and loss occur successively in DL and because the values compared are divided by diffraction probability. The normalized intensities of the inelastic scattering at peak energies of elastic intensity are extracted and redrawn in Fig. 8-2-5 as dots.

EELS cross sections of various excitations were calculated according to eqs. (8-1-4, -5,-6), where q_c's for plasmons of $MoSe_2$ and Ag were estimated from

$$\frac{\hbar^2}{2m}\left((q_c + q_F)^2 - q_F{}^2\right) = \Delta E, \qquad (8\text{-}2\text{-}1)$$

where q_F's are the Fermi wave numbers obtained from the size of the Brillouin Zone [10] and Fermi velocity [12] for $MoSe_2$ (2.21Å^{-1}) and Ag (1.20Å $^{-1}$), respectively. In $MoSe_2$, which is a n-type semiconductor, ΔE in eq. (8-2-1) was subtracted with the band gap (~1.6eV). The results of the calculation are indicated in Figs. 8-2-4 and -5 as solid lines where the scale of the ordinate were determined by the least square fitting.

The calculated loss probability deviates from the experimental results differently depending upon the sort of excitations. First we analyze the plasmons of $MoSe_2$, for which L process is forbidden because of the cut-off wave number. The possible factors determining the deviation are the dimension of the material and the duration of interaction (Δt). Since $MoSe_2$ has the layered structure, the dispersion curve of plasmon will not cross that of one electron excitation in the direction perpendicular to the layers, and consequently the cut off wave number should be longer than the ordinary material. However, this effect will work less strongly for higher ΔE, because at higher kinetic energy the electron is nearer to the three dimensional free electron state. Therefore, we have chosen the bulk plasmon (ΔE=24eV) to derive Δt. The experimental result was divided by the calculated probability to obtain the E_p dependence of Δt. Then the probing depth (Δl) was calculated by $\Delta l = v\,\Delta t$, where v is the velocity of the electron proportional to $\sqrt{E_p}$. The result is shown in Fig. 8-2-6 as dots.

Since it is commonly considered that the probing depth of REELS is proportional with the mean free path of the electron inside the solids determined mainly by the bulk-plasmon excitation, calculation according to eq.(8-1-4) is shown in Fig. 8-2-6 as a solid line after adjusting the scale to produce the best fit. The two curves disagree considerably at the lowest E_p region. This result can be explained by considering the effect of the probability of back-scattering diffraction. Let us make a one-dimensional model in which electrons travel along +x or -x direction. An incident electron runs in the +x direction, and the electron changes its direction to -x by the diffraction which occurs with the probability of $1/\lambda_D$ per unit length. The electrons are absorbed by successive energy loss process with the probability of $1/\lambda_L$ per unit length. Multiple diffraction is neglected. With this model, the total reflectivity (R) and the average penetration depth of the returning electrons (d) are calculated as follows.

$$R = 1/(1+2\lambda_D/\lambda_L) \qquad (8\text{-}2\text{-}2)$$

$$d = (1/\lambda_D+2/\lambda_L)^{-2} / \lambda_D \qquad (8\text{-}2\text{-}3)$$

The factor 2 comes from the loss probability in the round trip of electrons. It follows from eq. (8-2-3) that

$$\text{if } 1/\lambda_D << 1/\lambda_L,\ d \approx \lambda_L^2/4\lambda_D \qquad (8\text{-}2\text{-}4a)$$

$$\text{if } 1/\lambda_D >> 1/\lambda_L,\ d \approx \lambda_D. \qquad (8\text{-}2\text{-}4b)$$

Therefore the diffraction process cannot be neglected anyway. Detailed experimental analysis with angle resolution is expected to clarify this problem quantitatively.

As for Ag, the feature of free electron plasmon at 3.4 eV agrees well with that of surface plasmon at low E_p region, which is consistent to the results of the inelastic LEED study [13]. At high Ep region, the roughness of the film surface is probably involved in the difference between the experiment and the calculation. The experimental intensity of bulk-plasmon is considerably larger and smaller than the calculation above 300eV and below 150 eV, respectively. The former is explained by the probing depth as discussed above, while the latter

is probably because a large portion of electrons are lost by the surface plasmon before being scattered by the bulk plasmon.

Lastly, let us discuss the possibility of "electron energy loss holography" by using the above understanding of the processes. The calculation for Se(3d) core level is considerably smaller than the experimental results below E_p~200eV, which is not observed for plasmons. The reason is probably because the back-scattering loss probability (L) is more pronounced at lower E_p while it is forbidden for plasmons because of the cut-off. It is probably meaningful to investigate the interference of electrons after L process at these low E_p's with an angle resolved spectrometer. However, the primary energy must be low for the strong L and LD intensity. It must be noted that the selection of atomic species is then problematic because analysis for the low energy electrons is difficult due to the strong multi-scattering. The conclusion from the present analysis is that "energy loss holography" might be possible, although the selection of atomic species is strictly limited because of the competition between the energy loss (L) process and back-scattering diffraction.

8-3. Conclusion and outlook

Incident energy dependence of the electron energy loss intensity was measured in the reflection geometry using a double-pass CMA in order to clarify the processes involved experimentally. The back-scattering energy loss process becomes important in core level excitations at low incident energy, while it is forbidden for the plasmons with the energy range of CMA. By analyzing the bulk plasmons in $MoSe_2$ the probing depth was derived, from which it is noticed that the elastic diffraction process in the probing depth is important. The feature of surface and bulk plasmons in Ag epitaxial films were in good agreement with the theory. Detailed angle resolved analysis will be useful to understand the mechanism of depth-profiling and study the feasibility of EELS analogue of electron emission holography.

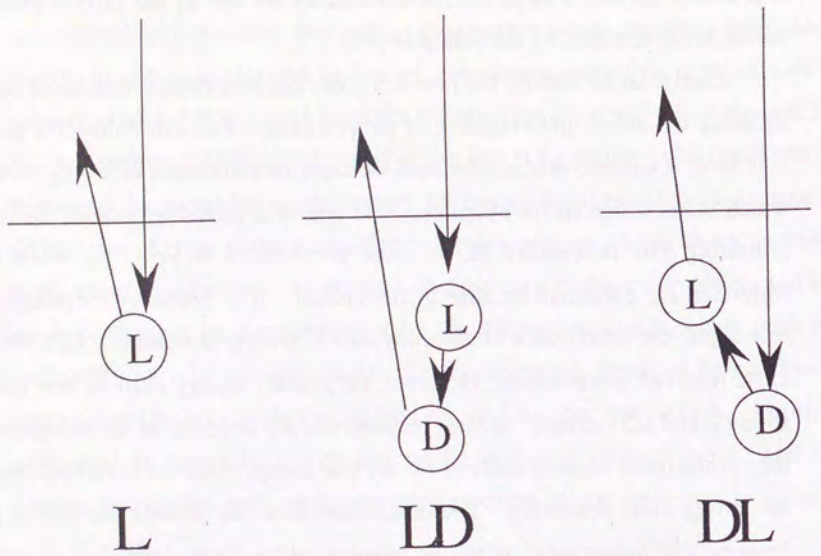

L : Inelastic scattering (Energy Loss)

D : Elastic Scattering (Diffraction)

Fig. 8-1-1: A schematic diagram of processes of REELS. "L" is back-scattering loss process, "LD" and "DL" are "forward-scattering loss before back-scattering diffraction" and "back-scattering diffraction before forward scattering loss", respectively.

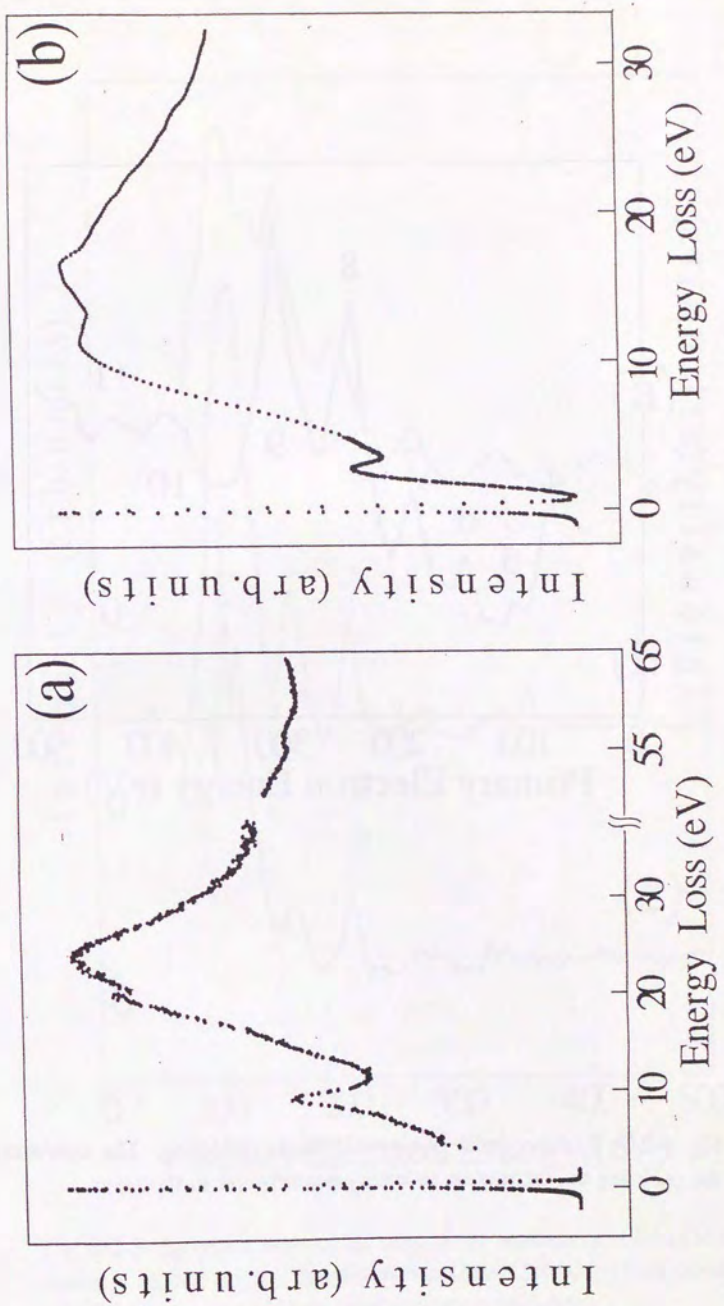

Fig. 8-2-1: EELS of (a) $MoSe_2$ (0001) and (b) Ag (111) epitaxial film. E_p=300eV.

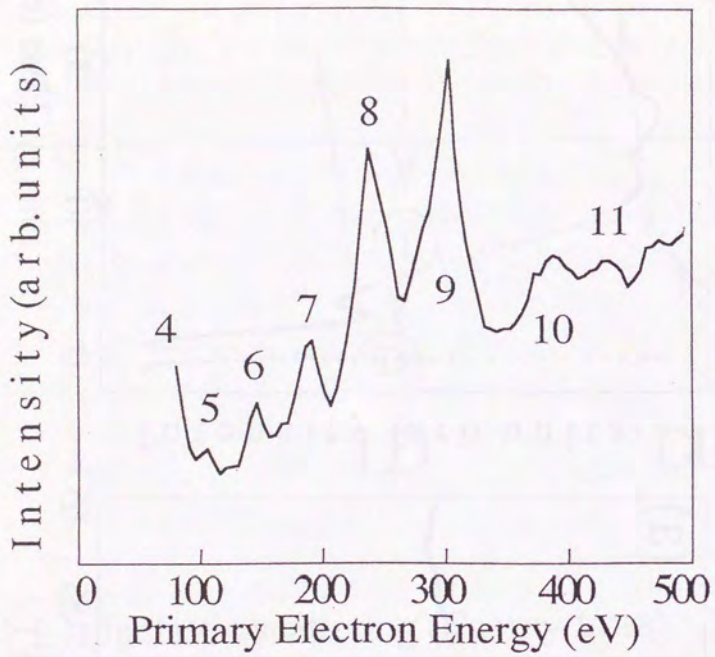

Fig. 8-2-2: E_p dependence of elastic intensity of $MoSe_2$. The numbers at the peak are the diffraction indexes perpendicular to the layer.

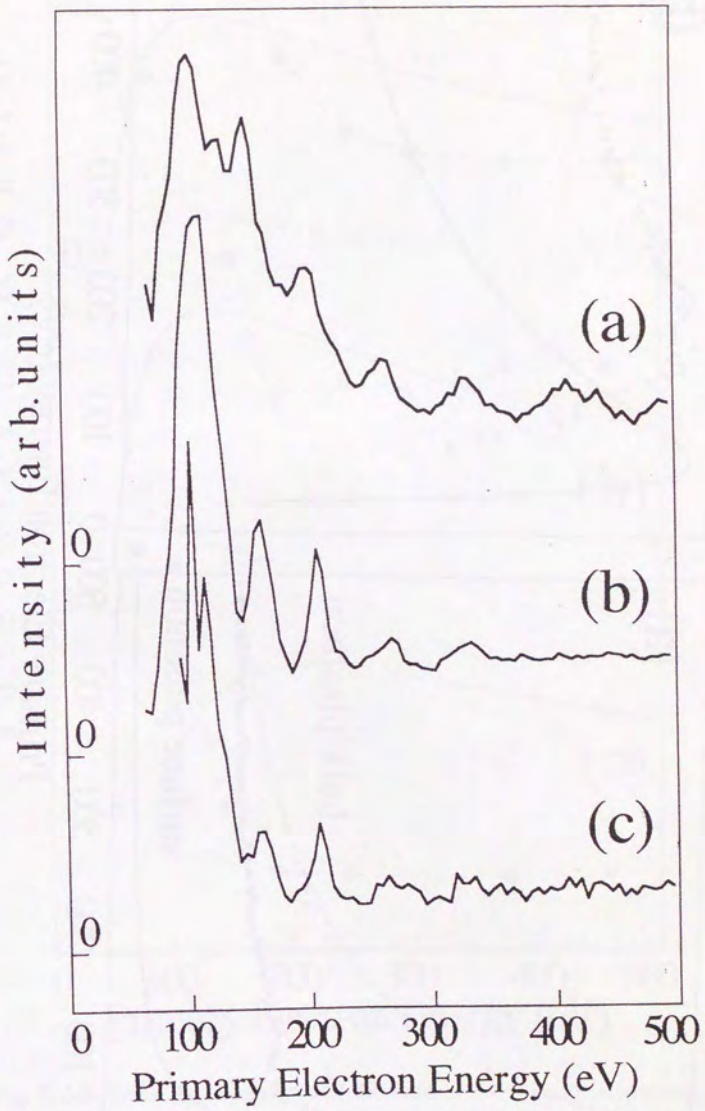

Fig. 8-2-3: E_p dependence of the ratio of the inelastic scattering to the elastic of $MoSe_2$ (0001). (a) π-plasmon ($\Delta E \sim 8.5$eV), (b) bulk plasmon ($\Delta E \sim 24$eV), (c) Se (3d) core level excitation ($\Delta E \sim 55$eV).

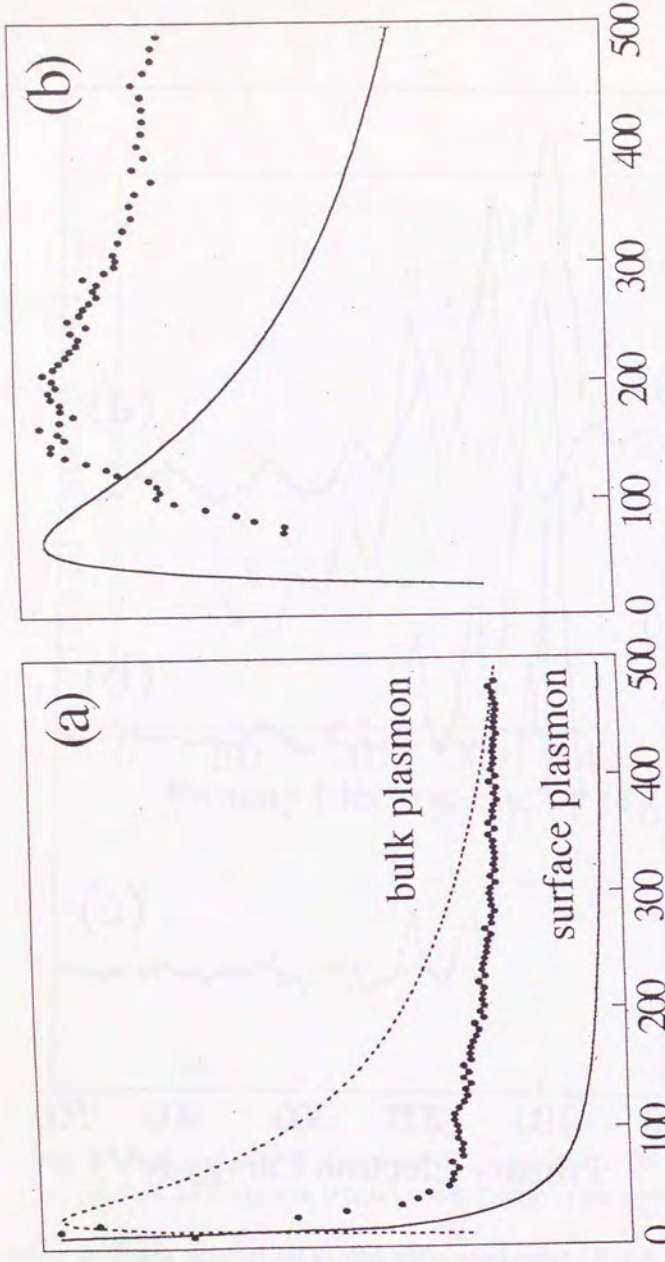

Fig. 8-2-4: Dots: E_p dependence of the ratio of the inelastic reflection to the elastic of Ag(111). Solid and dashed lines: E_p dependence of the calculated excitation probability. (a) free electron-plasmon (ΔE~3.4eV), (b) bulk valence plasmon (ΔE~17eV).

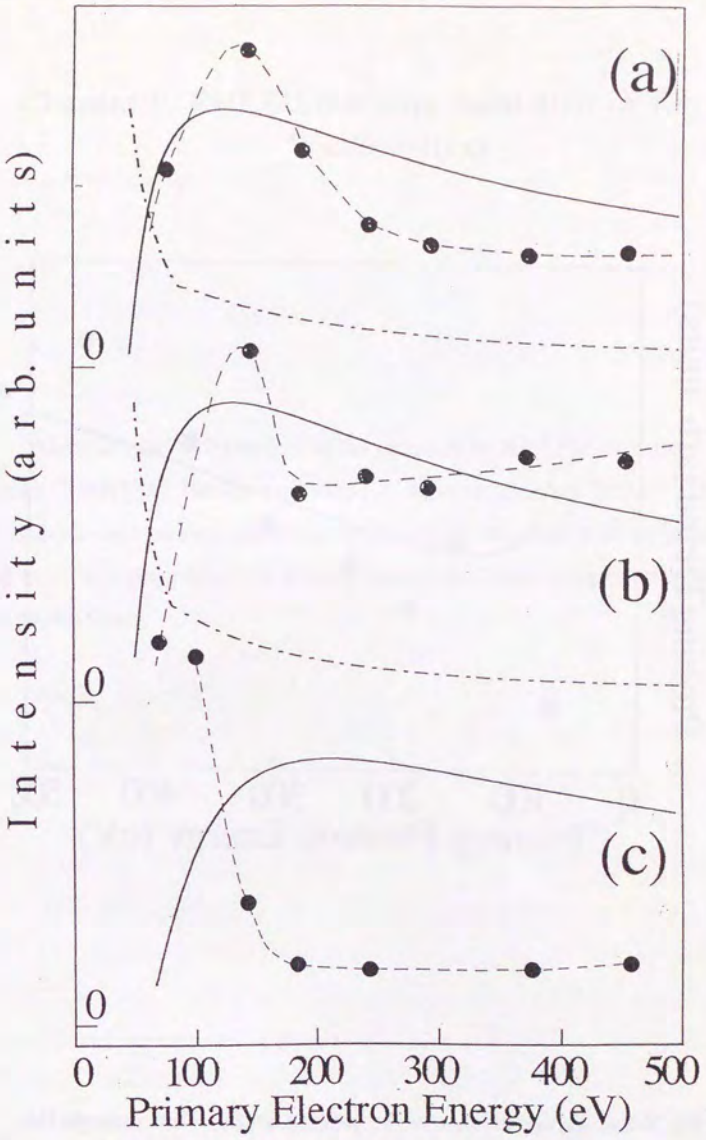

Fig. 8-2-5: Dots: E_p dependence of the ratio of the inelastic scattering to the elastic of $MoSe_2$ (0001) at DL-dominant energy. Solid Lines: E_p dependence of the calculated excitation probability. (a) π-plasmon (ΔE~8.5eV), (b) bulk plasmon (ΔE~24eV) , (c) Se (3d) core level excitation (ΔE~55eV).

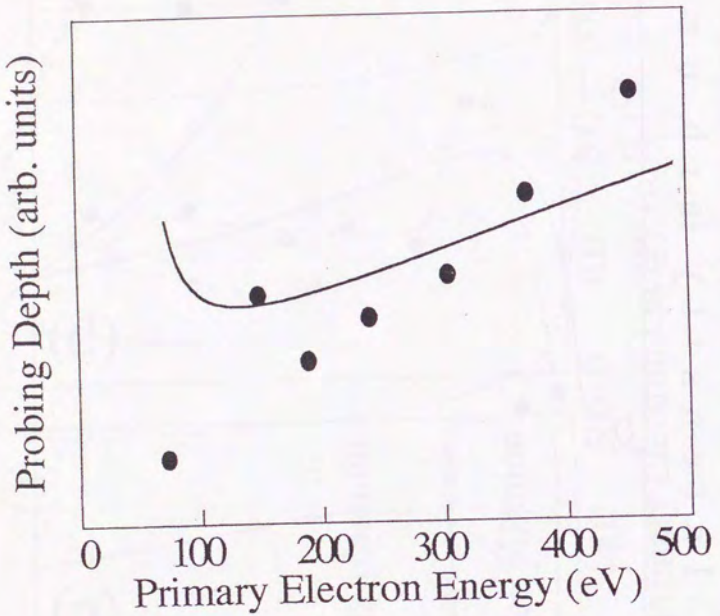

Fig. 8-2-6: E_p dependence of the probing depth. Dots indicate the experimental analysis obtained from the bulk-plasmon of $MoSe_2$, and a solid line is obtained from the calculation assuming the inelastic scattering is the determining factor.

Chapter 9. RHEED intensity oscillation in van der Waals epitaxy

Oscillations of diffracted beam intensity in RHEED have been observed during VDWE of $NbSe_2$ and $MoSe_2$ on Se-terminated GaAs($\bar{1}\bar{1}\bar{1}$) surfaces. Monolayer- and bilayer- mode oscillations were observed at different diffraction points. The existence of the bilayer- mode oscillation suggests the polytype of the grown films.

9-1. Introduction

It has been reported that periodic variations occur in the intensity of reflection high energy electron diffraction (RHEED) patterns during molecular beam epitaxy (MBE). The oscillatory behavior is believed to indicate two dimensional layer-by-layer growth. Historically, they were first observed in GaAs [1] and (Al, Ga)As [1,2]. The bilayer-mode oscillation was first reported on Si for certain diffraction points [3]. Although RHEED oscillation has been observed for several materials, so far, no report is available on layered materials. Therefore I have examined the time dependence of the RHEED patterns during VDWE. A system consisting of a video camera and a personal computer was constructed for the experiment. The growth of $NbSe_2$ and $MoSe_2$ (MX_2) films on Se-terminated GaAs($\bar{1}\bar{1}\bar{1}$) was investigated.

9-2. Experimental

The substrate used were Si-doped n-type GaAs($\bar{1}\bar{1}\bar{1}$) wafers because they have much flatter surfaces than other possible substrates for VDWE. The substrate was rinsed in acetone just prior to introduction into the growth chamber. The surface was cleaned by heating in ultrahigh vacuum. Although a halolike RHEED pattern was seen before heating, a (1 x 1) streak pattern appeared as the temperature increased to 300°C or more. The pattern showed sixfold rotational symmetry around the axis normal to the surface. Just after the streak pattern appeared, the heater was turned off to avoid surface roughening and arsenic depletion. Then a selenium beam was irradiated on the surface in order to terminate the dangling bonds of the surfaces with selenium atoms [4].

The MBE system used in the present experiment is described in detail in chapter 2. The base pressure of the growth chamber was 1 x 10^{-8} Pa. Purified selenium was evaporated from a Knudsen cell. Electrostatic focusing electron beam evaporators were used for evaporating niobium and molybdenum. The acceleration voltage of RHEED was 20 kV. The incidence angle of the electron

beam on the surface was less than 1°. The thickness of the grown film was measured by a profilometer after the specimen was taken out from the growth chamber.

A system consisting of a low-light video camera and a personal computer has been constructed in order to carry out a quantitative analysis of RHEED intensities. The video camera was set about 5cm in front of the phosphorescent screen. Video signals were put into the graphic interface board VDB-980E (OS-systems) and digitized in 6-bit data of 200 x 256 pixels. In order to improve the S/N ratio, data for a diffraction point were measured by averaging the digitized data for 3 x 3 pixels around it. The computer program was used primarily to analyze the data recorded in the video cassette tapes. The RHEED intensities can be measured in as many as ten selected areas per second in this system. Careful choice of proper diffraction points is needed because prominent oscillations can be observed only for specific points, as will be discussed later. The system is also applicable for real time analysis during growth.

9-3. Results and discussions

The RHEED pattern for Se-terminated GaAs substrate decayed after opening the shutter for the molecular beams. Eventually, new streaks of MX_2 (0001) appeared and were completed when about one unit layer had grown. The RHEED patterns for various azimuths showed that the films are rotationally commensurate with the substrate; that is, the edges of two-dimensional hexagonal lattices of the grown film and that of the substrate align with each other. The observed interval of streaks for the grown MX_2 coincided with the one expected from its own lattice constant. Those streaks persisted during further deposition and no apparent change in the intensity was seen by the naked eye. Observation by video camera, however, revealed that the intensities of certain diffraction points change with a long period from tens of seconds to several minutes. There

seem to be several incident azimuths which give prominent oscillation. The angle +18° off from the MX_2 [1000] axis was chosen among those azimuths.

Figure 9-3-1 shows the oscillations of intensity in the RHEED pattern during the growth of $NbSe_2$ at 620°C. The observed points were the specular and (1,0, 11.5) ones in reciprocal coordinates of the 2Ha polytype. The specular beam intensity oscillates with a period of 38 s, coinciding with the time for the growth of a unit layer estimated by thickness measurement. On the other hand, an oscillation with a period of 76 s was observed for (1,0,11.5), which is exactly the growth time of two layers. The oscillation amplitude was 5-10% of the whole diffraction intensity for both points.

It is interpreted that monolayer-mode oscillation of the specular beam is caused by the periodic change in density of monolayer steps at the top surface [2]. As for the bilayer period at (1,0,11.5) , it is considered to be related to the stacking structure of the grown films. Fig. 9-3-2 shows the structural polytypes of $NbSe_2$. First let us investigate the possibility of 2Ha polytype. Diffraction intensities for 2Ha-type $NbSe_2$ have been calculated kinetically. It is sufficient in the calculation only to consider two layers forming a unit cell of 2Ha- $NbSe_2$ because RHEED predominantly reflects the structure of the surface portion of the specimen. Then two inequivalent layer configurations are conceivable, which are described as A and B in Fig. 9-3-2. For the A and B configurations, the intensities on the (10) rod were calculated as shown in Fig. 9-3-3 (a) and (b), respectively. The calculation of intensity I was performed by the following formula:

$$I = \left| \sum_i f_i e^{ik \cdot r_i} \right|$$

$$= \left| f_{Se}(1+e^{2\pi i s z^*}+e^{2\pi i(\pm(2/3)+(1/2)z^*)}+e^{2\pi i(\pm(2/3)+((1/2)+s)z^*)}) \right.$$

$$\left. + f_{Nb}(e^{2\pi i(\pm(1/3)+(s/2)z^*)}+e^{2\pi i(\pm(1/3)+((1/2)+(s/2))z^*)}) \right|^2$$

where the upper and lower signs correspond to A and B configurations, respectively, and s = 3.36Å / (2 x 6.27Å). Here i represents an atom in a unit cell, r_i is the position of the atom i, f_i is the atomic scattering factor, and k=(1,0,z*) is a reciprocal vector. The atomic scattering factor was assumed to be proportional to the atomic number.

The A and B configurations alternately form the top surface while 2Ha-$NbSe_2$ is grown. In order to find out the diffraction point giving maximum intensity change, the difference of curves Fig. 9-3-3 (a) and (b) is plotted in Fig. 9-3-3 (c). As shown in the figure, the maximum intensity change will be seen at z*=11.5. This result is consistent with the observation that bilayer mode oscillation was observed strongly at (1, 0, 11.5) diffraction point. According to Fig. 9-3-3(c), a prominent bilayer mode oscillation is also expected near the (1,0,3.5) point. Nevertheless, it has not been obtained in the present experiment. It can be explained from the fact that the intersection of the 10 rod with an Ewald sphere is around (1,0,11) in the present experimental set up. As shown above, the experimental result is explained well if the 2Ha- type is grown. We can easily eliminate the possibility of the 2Hb- and 3R-type because no change in the surface structure is expected in the growth of these polytypes. However, since 4Ha is constructed with two 2Ha-like stackings (A', B' in Fig. 9-3-2) and two 2Hb-like stackings (C, D in Fig. 9-3-2), one might suspect that the 4Ha type also shows the bilayer-mode oscillation. In order to clarify this point, we have calculated the intensities I_x from configuration x in Fig. 9-3-2 (x=A',B',C,D).

The method of calculation was as shown above for the 2Ha type. The results for $z^*=11.5$ are as follows (they are normalized by $I_{B'}$):

$$I_{A'}=0.020;\quad I_{B'}=1.000;\quad I_C=0.952;\quad I_D=0.068.$$

These values indicate that the 4Ha type will show the quadrilayer-mode oscillation, but not bilayer-mode oscillation. It can be concluded that $NbSe_2$ film showing the oscillation in the present experiment is 2Ha-type.

The strong bilayer oscillation observed in the present experiment indicates that the antiphase portion is considerably small. In other words, one of the A or B configurations forms a dominant portion of the top surface at one time. This arises from the following facts: 1) RHEED sees the broad region of the sample surface; 2) if there nearly the same amount of A and B configurations exists on the top surface, the bilayer oscillation will be canceled. The generation of the antiphase portion may be suppressed by the following mechanism. Although the top surface of Se-terminated GaAs($\bar{1}\bar{1}\bar{1}$) has sixfold symmetry, the symmetry is reduced to threefold symmetry if the underlying second layer is taken into account. Then one of the A or B configurations is more favorable energetically as the first grown layer of $NbSe_2$ on Se-terminated GaAs($\bar{1}\bar{1}\bar{1}$) surfaces, which will reduce the antiphase portion.

The RHEED intensity variations during growth of $MoSe_2$ are shown in Fig. 9-3-4. The substrate temperature was 620°C. The observed points were specular and (1,0,11.5) ones. The observed periods of oscillation were 34 s and 68 s. Nearly the same conclusion can be deduced for the growth of 2H-$MoSe_2$, following the similar discussion to that shown above. It is noticeable that the bilayer-mode curves have different shapes for $NbSe_2$ and $MoSe_2$. The former is almost sinusoidal, while the latter is truncated. It may reflect some difference in the growth mechanism.

9-4. Comparison with GID results in chapter 5

In the present research, the structure of the $NbSe_2$ films has been measured also with grazing incidence x-ray diffraction (GID). The result of GID analysis was that $NbSe_2$ films grown Se-GaAs were 2Ha and mixture of 2Hb and 3R, depending on the temperature. The growth temperature examined in the study of RHEED oscillation is 620°C, which is nearer to the condition in GID for 2Ha (535°C) than that for 2Hb+3R (420~500°C). Hence the result of this chapter is consistent with that of GID. It was also found that the Bragg rod profile in GID had sixfold rotational symmetry for all of the growth temperatures, whereas antiphase portion of the alternating layers was small in RHEED oscillation. These are not conflicting with each other because Bragg rod profile of 2Ha-type in GID has almost sixfold symmetry because of the relatively large probing depth of x-ray (more than 2 monolayers). In this sense, the analysis in this chapter is complementary to GID.

9-5. Conclusion and outlook

The RHEED oscillations have been observed during the MBE growth of $NbSe_2$ and $MoSe_2$ on Se- terminated GaAs($\bar{1}\bar{1}\bar{1}$) substrates. Two kinds of periods, corresponding to the growth of one unit layer and two unit layers, have been observed at different diffraction points for both $NbSe_2$ and $MoSe_2$. The existence of bilayer-mode oscillation indicates that 2H-type $NbSe_2$ and $MoSe_2$ have been grown with very small antiphase portions. The present RHEED oscillation will open a way for the precise control of thickness of the grown films. However, the weak amplitude of the oscillation intensity at present (5~10%) indicates only a small portion of the film follows the layer-by-layer growth mode. Improvement of the growth condition for the better crystallinity of the grown films will be achieved by searching the conditions which enhances the oscillation amplitude.

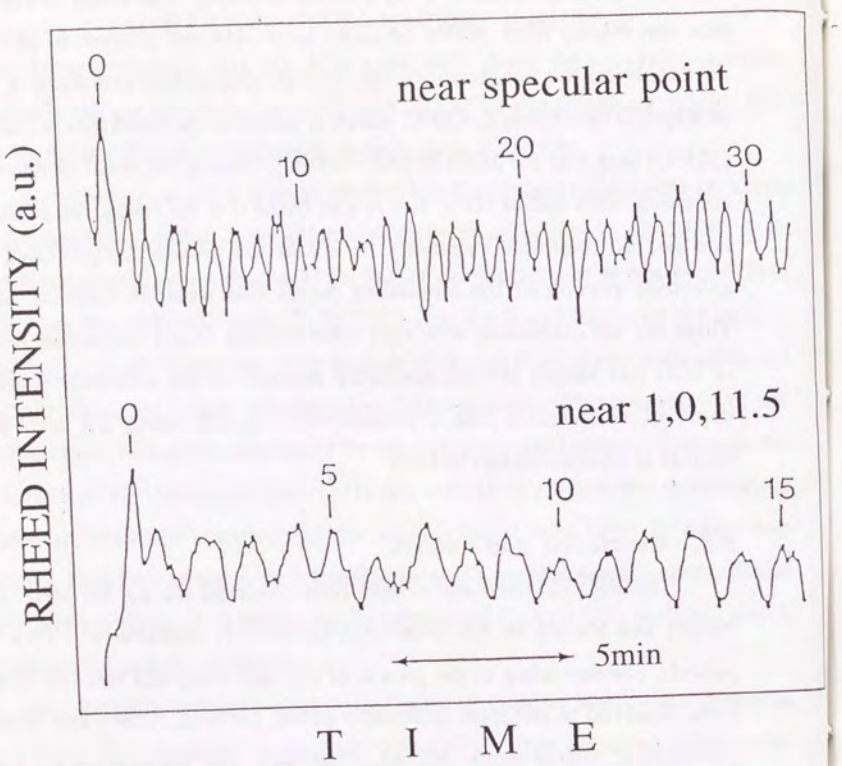

Fig. 9-3-1: RHEED oscillation observed during MBE growth of $NbSe_2$ at 620°C. The periods of oscillations in the upper and lower curves are 38 s and 76 s, respectively.

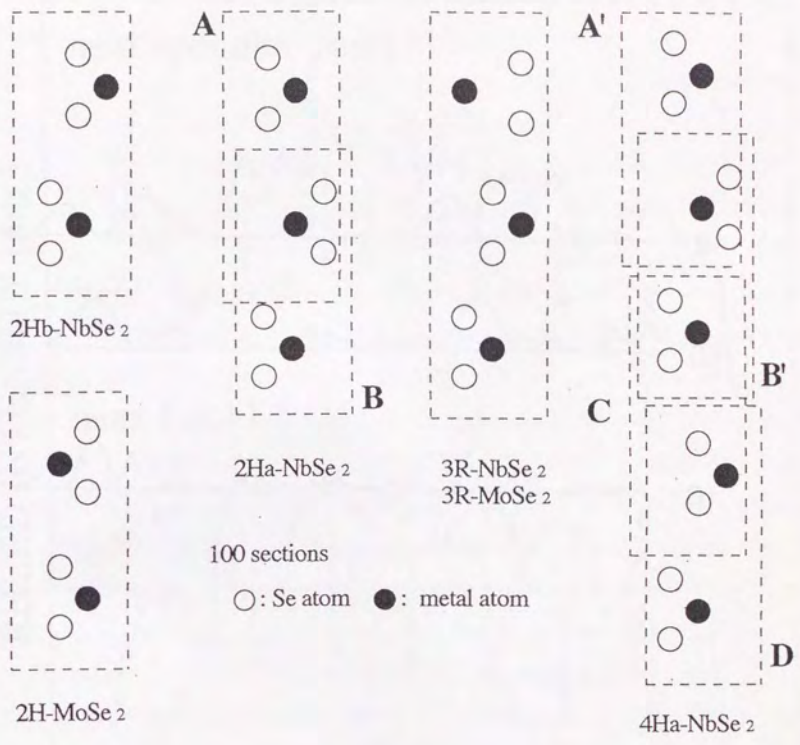

Fig. 9-3-2: 100 sections of the polytypes of $NbSe_2$ and $MoSe_2$.

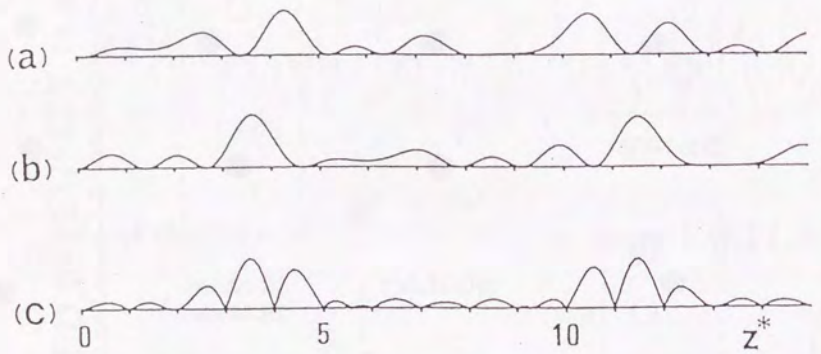

Fig. 9-3-3: Curves (a) and (b) are the diffraction intensities along the (10) rod calculated for a unit cell of 2Ha-$NbSe_2$ in A and B configurations, respectively. Numbers z* below the abscissa indicate the third coordinate (perpendicular to the surface plane) of the reciprocal lattice. Curve (c) shows the difference of curves (a) and (b).

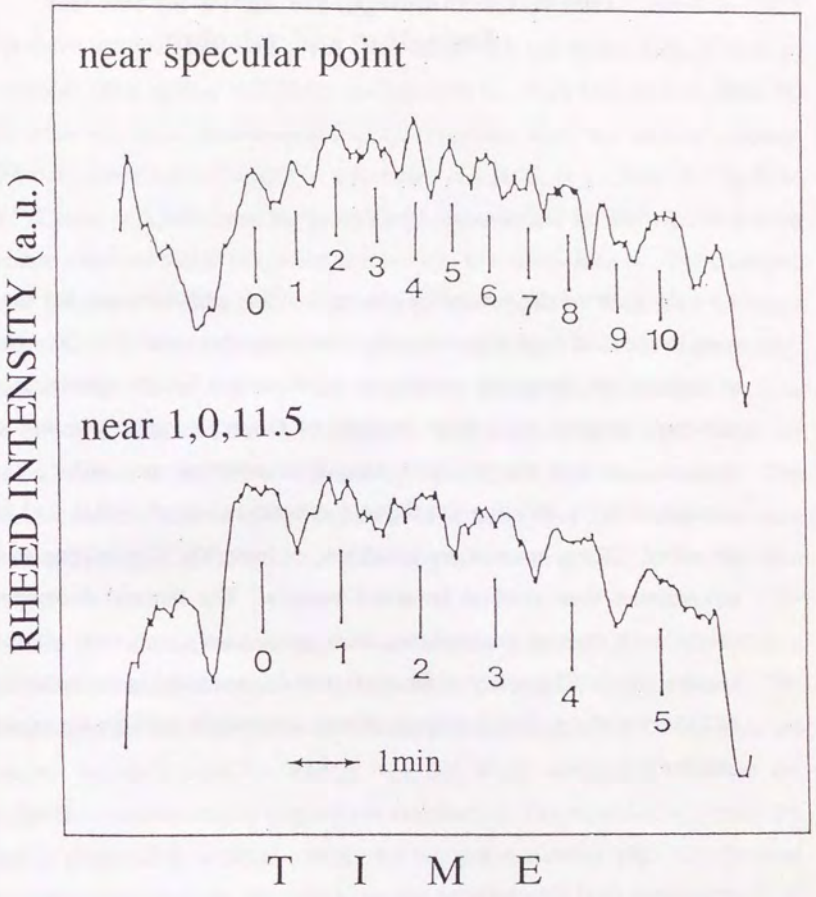

Fig. 9-3-4: RHEED oscillaiton observed during the MBE growth of $MoSe_2$ at 620°C.

Chapter 10. Thermal decomposition of SnS_2 and $SnSe_2$: Novel molecular-beam epitaxy sources for sulfur and selenium

In most of the preceding chapters, sulfur and selenium for the VDWE were evaporated from Knudsen-cells containing elemental S or Se. Those kind of sources are, however, sometimes inconvenient for the operation with the ultrahigh vacuum equipment because of the high vapor pressure of those elements. In this chapter, new sources of selenium and sulfur in ultrahigh vacuum (UHV), utilizing the thermal decomposition of $SnSe_2$ and SnS_2, are described. These sources are bakable to at least 300°C providing much more convenience than element Se and S sources. The thermal decomposition is studied with thermal gravitometry, mass spectrometry, and x-ray photoemission spectroscopy. The utility of the sources is demonstrated in the epitaxial growth of $TiSe_2$ on MoS_2. The $SnSe_2$ source was successfully used for the experiment in chapter 7.

10-1. Introduction

The need for a clean and high flux of sulfur and selenium in UHV deposition systems has been greatly increased with the recent development of molecular beam epitaxy (MBE) for chalcogenide materials such as ZnS, ZnSe [1] and transition metal dichalcogenides [2]. Previous work has utilized a source with pure elemental chalcogen in a Knudsen cell [1,2], or gaseous H_2S or H_2Se [3]. Elemental chalcogens are particularly inconvenient in the vacuum system because these elements evaporate at relatively low temperatures. For example, vapor pressures of sulfur and selenium are 1 mtorr at 183.8°C [4] and 1.7 mtorr at 200°C [5], respectively. A common practice, to avoid unnecessary contamination due to high vaporization pressure during the system bakeout, is to use either a linear translation mechanisms to draw the source back out of the baking media, or to reduce the baking temperature near the sources. The gaseous sources also have the additional disadvantage of producing enormous residual hydrogen in the system, which may affect the growth of the thin film [6].

In this article we introduce novel sources for chalcogens in which a thermal decomposition of tin dichalcogenides, SnS_2 or $SnSe_2$, is utilized. Tin dichalcogenides have the following favorable characteristics: (a) Compounds are layered materials with low energy van der Waals surfaces [7], thus are minimally contaminated by exposure to ambient air. (b) Pure single crystals are readily prepared in a large quantity by Bridgman method [8]. (c) Thermal decomposition of these compounds occurs at relatively high temperatures, in particular, higher than common baking temperatures of the MBE systems.

The thermal decomposition of tin dichalcogenides have been investigated first by thermal gravimetric analysis (TGA), mass spectrometry, and x-ray photoelectron spectroscopy (XPS). The utility of this chalcogen source has then been demonstrated by fabricating $TiSe_2$ epitaxial films on MoS_2.

10-2. Experimental

SnS_2 and $SnSe_2$ were prepared in a large grain (3-5mm) polycrystalline form by the Bridgman method. Details are found elsewhere [8]. The TGA analysis was performed by heating the sample at the constant rate of 10 °C / min and following its weight as a function of temperature. The evolution of chalcogen species from the compound was then characterized isothermally at various temperatures with mass spectrometry. From these experiments the activation energy was determined. For the thermal decomposition experiments approximately 100 mg of SnS_2 or $SnSe_2$ was contacted to a Mo heater. To avoid temperature inhomogeneity in the sample, the surface was further covered with a thin tantalum foil with a small hole, from which the decomposition species escaped and subsequently were detected in a line of sight by the mass spectrometer. The temperature was calibrated with several thermocouples placed at various points and had a temperature variation of less than ±10°C. The flux of the various species was determined from their mass spectral peak heights. The partial pressure of detected chalcogens ranged from $1x10^{-6}$ Pa to $5x10^{-4}$ Pa. The mass resolution of the spectrometer (UTI-100) is 1 atomic mass unit (AMU). Changes in the stoichiometry of source materials were checked with XPS. For this experiment, the specimen was heated in the separate vacuum chamber, which is connected to the XPS system, until thermal equilibrium was achieved. After each heating step the specimen was transferred to the XPS chamber, an ion-pumped UHV chamber with a base pressure of $3x10^{-8}$ Pa. The XPS spectrometer was a Surface Science Laboratory's ESCA-100 with the energy resolution 0.8 eV in FWHM (calibrated with Au(4f)).

10-3. Results and discussions

10-3-1 SnS_2

The change of the sample weight with temperature during heating at the rate of 10 °C/min is shown in Fig. 10-3-1. There are three plateaus in the TGA,

below 550°C, around 740°C, and above 920°C. The residual weight at the first plateau is 82% of the original, which is equivalent to the molecular weight ratio of SnS to SnS_2 (82.5%). The second plateau is at 46%, which corresponds to 2/3 of molecular weight of Sn with respect to SnS_2 (43.3%). Hence, the decomposition processes suggested from TGA are:

$$SnS_2 \rightarrow SnS + S\uparrow \quad (550 - 740°C). \qquad (10\text{-}1)$$

$$3SnS \rightarrow 2Sn + SnS_3\uparrow \quad (740 - 920°C). \qquad (10\text{-}2)$$

Equation (10-1) was partly verified by the results from XPS measurements after SnS_2 was heated to 650°C (Fig. 10-3-2). The ratio of S to Sn starts decreasing at 500°C. The 1:1 stoichiometry of Sn : S is observed above 570°C through the first decomposition process (Eq. (10-1)). When SnS_2 was heated to 900°C, the evolution of SnS_3 was confirmed by mass spectrometry (Fig. 10-3-3) from the appearance of a strong peak at 215 AMU. In general, single crystals of metal dichalcogenides can be grown by vapor transport, in which excessive chalcogen can be used as a transport agent [9]. The SnS_3 found in this experiment may be the responsible chemical species in the self transport of SnS_2. The activation process for the reaction (10-1) was determined by mass spectrometry. The peak at 64 AMU (S_2^+) rather than 32 AMU (S^+) was chosen to represent the sulfur species, since this peak has no interference from possible contaminants such as oxygen or hydrocarbons. While the temperature was raised isothermally, no decay of the flux was observed at the measured temperatures. The peak heights versus temperatures are then plotted in Arrhenius plot as shown in Fig. 10-3-4. The error bars in the peak height are estimated by fluctuation between several experiments, while those in the temperatures are only ±10°C. The activation energy of reaction (10-1) is calculated to be 6.9±0.1 kcal / mol from the slope of the plot in Fig. 10-3-4. The good linearity of the Arrhenius plot appears to show that only reaction (10-1) is involved at this temperature range. No tin was detected by the mass spectrometer below 600°C.

10-3-2 $SnSe_2$

XPS of the sample kept at 350°C for one day shows the 1:1 stoichiometry of Sn : Se, which indicates the first stage decomposition of $SnSe_2$ is as follows:

$$SnSe_2 \rightarrow SnSe + Se\uparrow. \qquad (10\text{-}3)$$

The TGA shows that the weight becomes constant at 25% of that of $SnSe_2$ after heating to 700°C. This value corresponds to 2/3 of the molecular weight ratio of Sn to $SnSe_2$ (28.6%), therefore, by analogy to SnS_2, the second stage appears to be

$$3SnSe \rightarrow 2Sn + SnSe_3\uparrow. \qquad (10\text{-}4)$$

TGA shows the first significant weight loss is at 340°C. The activation energy for the decomposition was measured with the mass spectrometer as described above. The peak at 160 AMU (Se_2^+) was chosen. The Arrhenius plot is shown in Fig. 10-3-5, in which error bars are larger than the cases of SnS_2 since the temperatures were much lower and the thermal equilibrium was very slowly attained. The activation energy is calculated 2.9±0.3 kcal/mol. Again no tin was detected by the mass spectrometer below 400°C.

The experiments shown above, the results of which are summarized in Table 10-1, suggest that SnS_2 and $SnSe_2$ decompose to produce reasonable S and Se flux above 550°C and 340°C, respectively. These temperatures are much higher than usual baking temperatures for most vacuum systems. Although the reactions are endothermic, there are upper limits in the source temperatures above which further decomposition produces Sn contamination in the flux.

Table 10-1: Liberation of chalcogen from SnX_2 (X=S,Se).

	$SnX_2 \rightarrow SnX+X$ (X=S,Se)		$3SnX \rightarrow 2Sn+SnX_3$
Compound	Starting temp(°C)	Ea(kcal / mol)	Starting temp(°C)
SnS_2	550	6.9±0.1	740
$SnSe_2$	340	2.9±0.3	above 400

SnS_2 and $SnSe_2$ have a layered structure composed of sheets of tin atoms sandwiched between hexagonally closest-packed sheets of chalcogen atoms. Since chemical bonds at the surface of these materials are saturated, they are minimally contaminated by the exposure to air. Considering those advantages, tin dichalcogenides can be useful for sources of chalcogen in Knudsen cells.

10-3-3 Growth of $TiSe_2$

To demonstrate the utility of these chalcogen source, $TiSe_2$ was grown epitaxially on the surface of MoS_2. Titanium was sublimed from a joule-heated ribbon, and selenium was evaporated form the $SnSe_2$ Knudsen cell. The cell was constructed from Pyrex glass and its shape is shown in Fig. 10-3-6. Three grams of crushed single crystalline $SnSe_2$ were contained. The temperature of the cell, which was monitored at the center of the cell with a *K*-type thermocouple, was kept at 370°C during the growth. The evaporation rate of titanium and selenium were about 0.3 and 6Å/min, respectively. The base pressure of the growth chamber was 2×10^{-7} Pa and the MoS_2 substrate was heated to 310°C during the growth. Reflection high energy electron diffraction (RHEED) was used to monitor the growth process. Good crystallinity with epitaxial relation to the substrate was observed by RHEED. Following growth, the sample was transferred to the XPS chamber under UHV condition for the analysis. Fig. 10-3-7 shows XPS spectrum which shows no tin peaks. Comparison to the spectrum from bulk single crystalline $TiSe_2$ is also shown. The two spectra are identical. The spectra are also indistinguishable from a $TiSe_2$ film made with an elemental Se source.

10-4. Conclusion and outlook

Thermal decomposition of $SnSe_2$ and SnS_2 was investigated to study their utility as chalcogen sources for thin film growth. The decomposition involves the following two stages for both materials: (1) liberation of chalcogen from

SnX_2 (X=S or Se) to leave SnX in the first step, and (2) decomposition into SnX_3 and Sn. The temperature range of SnS_2 and $SnSe_2$ to produce chalcogen are 550-600°C and 340-370°C, respectively. Those temperature are much higher than usual baking temperatures for most vacuum systems. The activation energy for these reactions are 6.9±0.1 kcal/mol and 2.9±0.3 kcal/mol, respectively. We have demonstrated these tin dichalcogenides can be utilized for chalcogen sources for the growth of epitaxial titanium diselenide thin films. This $SnSe_2$ source was also successfully used in chapter 7.

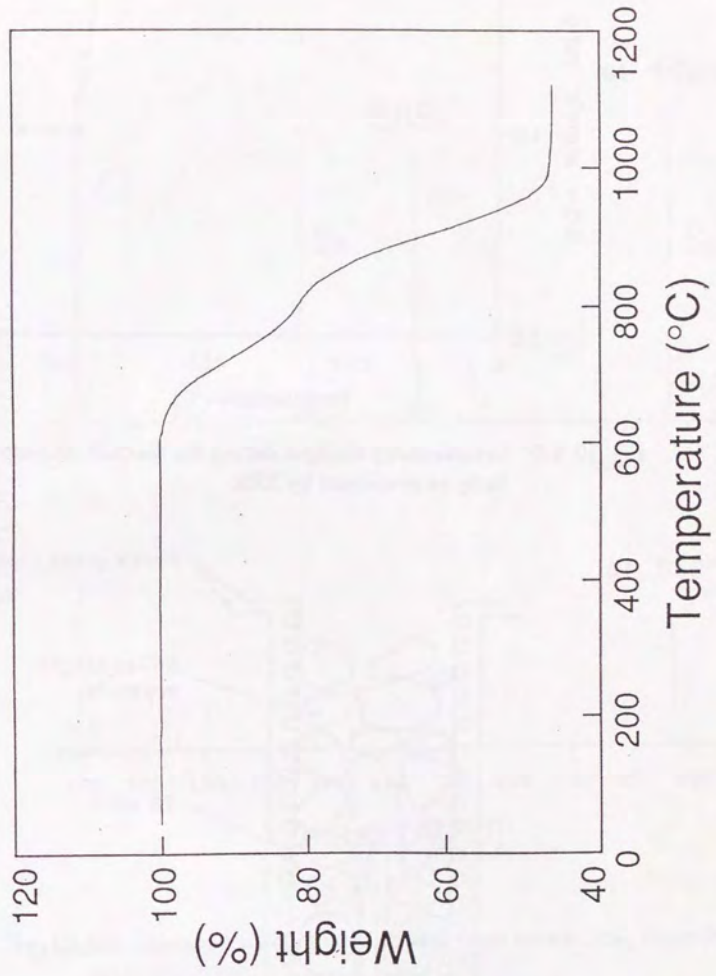

Fig. 10-3-1: TGA of SnS_2.

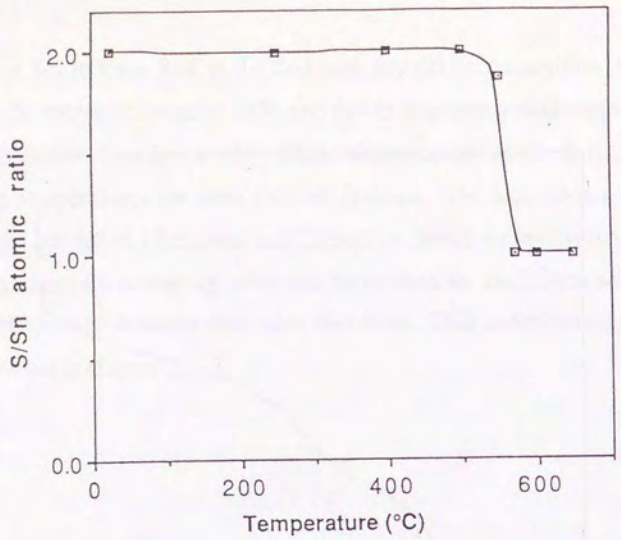

Fig. 10-3-2: Stoichiometry changes during the thermal decomposition of SnS_2 as monitored by XPS.

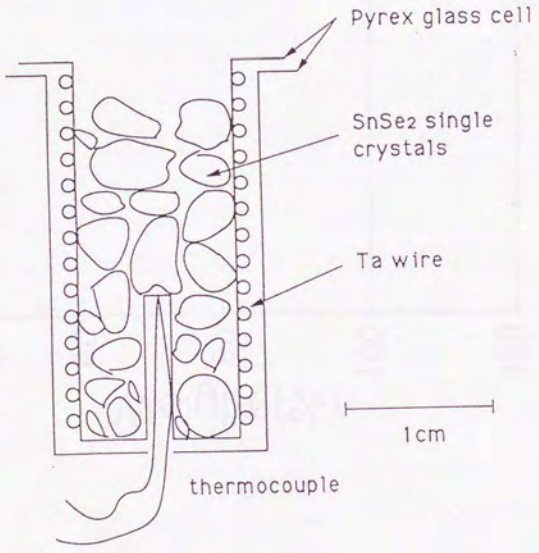

Fig. 10-3-6: Shape of $SnSe_2$ Knudsen cell.

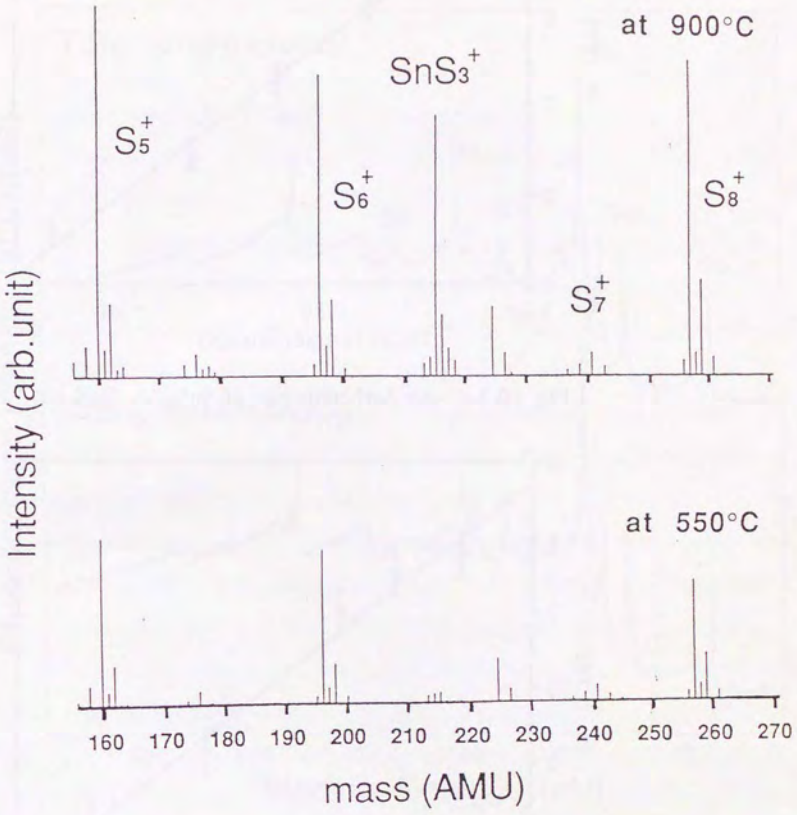

Fig. 10-3-3: Mass spectra of emitted species from heated SnS_2 (a) at 900°C (b) at 550°C.

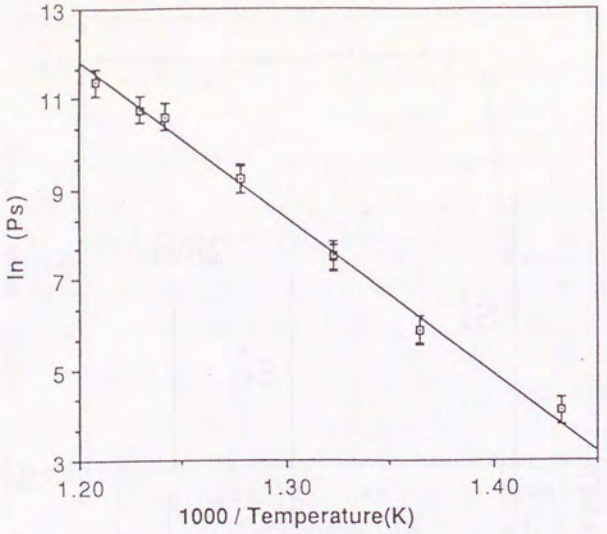

Fig. 10-3-4: An Arrhenius plot of SnS_2 -> SnS + S.

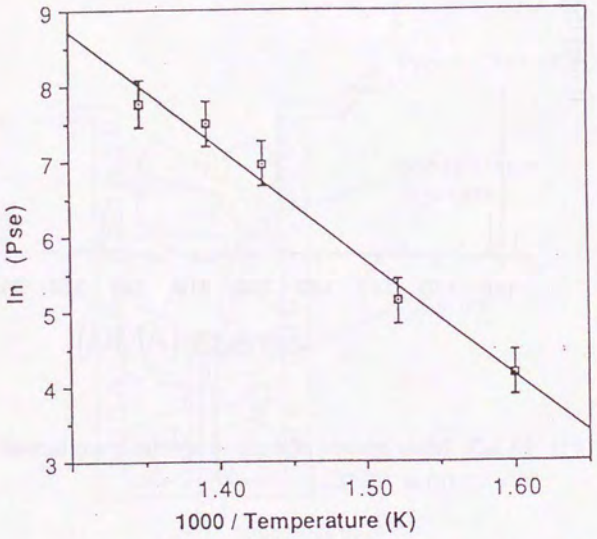

Fig. 10-3-5: An Arrhenius plot of $SnSe_2$ -> SnSe + Se

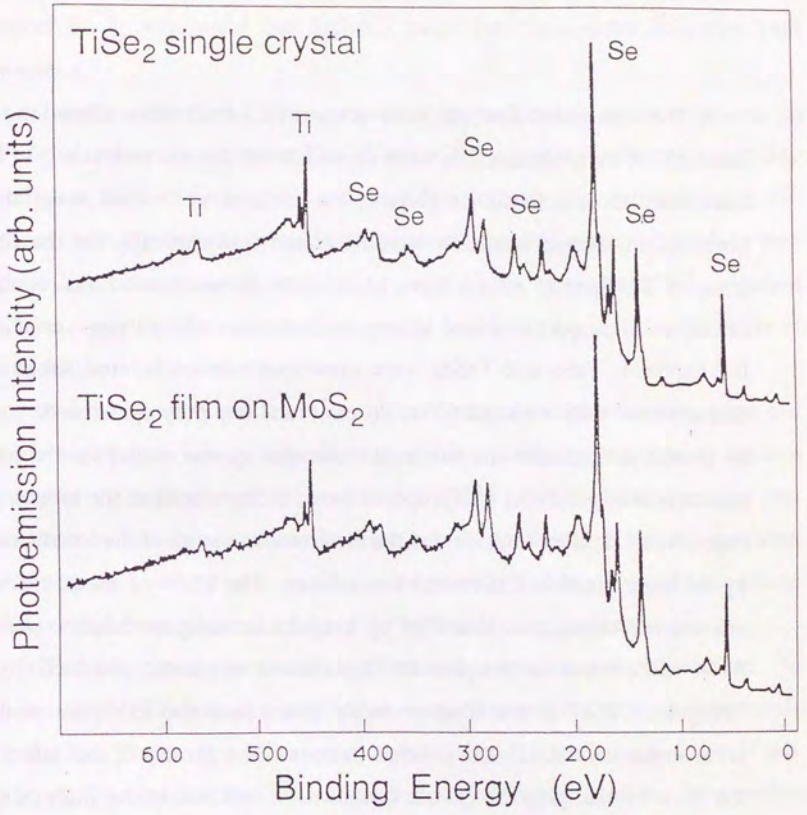

Fig. 10-3-7: XPS spectra of $TiSe_2$ single crystal and a epitaxial film grown on MoS_2 using $SnSe_2$ Knudsen cell.

Chapter 11. Summary and future prospects

The structures and physical properties of ultrathin films and hetero interfaces of layered materials were studied in the present research. In order to understand the electronic property of the surfaces of layered materials, work functions of layered materials were measured systematically for the first time (chapter 3). Special efforts have been made to understand and control two fundamental properties found among layered materials: polytypism and CDW. In chapter 4, TaS_2 and $TaSe_2$ were grown on various layered substrates and characterized with XPS and STM. It was found that polytypes can be controlled by growth temperature and substrate materials. A new model for the formation mechanism of polytypes was proposed based on the results of the monolayer film experiments. It takes into account the electrostatic energy of the interfaces caused by the work function difference of each layer. The CDW of ultrathin films with nm-order thickness was identified by irregular intensity modulation observed in STM and anomalous temperature dependence of electric conductivity. This "irregular CDW" in the films probably arises from the existence of distorted areas in the crystal. If it is possible to control the density of the defect sites in the films by changing the growth condition, it will lead to the study of CDW in three dimensional confinement.

In order to determine the structures of the films and interfaces, grazing incidence x-ray diffraction technique was applied to the epitaxial films of $NbSe_2$ and $TaSe_2$ with nm-order thickness (chapter 5). The structures were dependent on substrates and growth temperature, which indicates the polytype was controlled by those conditions. This result will be useful to elucidate the

mechanism of the epitaxy via van der Waals forces and to pursue novel physical properties in layered heteroepitaxial systems.

Metal-semiconductor interfaces of layered materials were studied in chapter 6. It was found that $SnSe_2$ / metal interfaces have Schottky limit properties.

Interface effect of CDW was studied by performing epitaxial growth on 1T-TaS_2 substrates (chapter 7). While CDW was not affected by $SnSe_2$ overlayers, XPS of $SnSe_2$ reflected the CDW transition in the underlying 1T-TaS_2. These concepts have not been proposed prior to the present work as seen from the fact that theoretical methods have not been established. It is expected that the present experimental approach will lead to a new field in the study of atomically controlled interfaces.

For the improvement of the analytical methods used for ultrathin films and interfaces, electron energy loss intensity was measured as a function of incident energy in the reflection geometry using a CMA. While electron energy loss spectroscopy has been used for the depth profiling analysis of hetero interfaces, the processes involved were not fully understood. It was revealed that elastic diffraction plays an important role in the back-scattering geometry.

The fabrication process of the films and interfaces was also studied. In chapter 9, RHEED intensity oscillations were observed in the layered materials for the first time. It confirms the layer-by-layer growth in van der Waals epitaxy. The existence of bilayer-mode oscillation provided the information concerning the polytypes of the grown film. In order to invent more convenient chalcogen sources for MBE, thermal decomposition of $SnSe_2$ and SnS_2 was studied in chapter 10. The reaction scheme was established and the utility as the MBE sources was demonstrated.

The approach taken in the present study - using controlled crystal growth and surface science techniques to investigate the fundamental physical and

chemical problems at interfaces - was fruitful. I expect the usefulness of this methodology in the following fields:

(i) Nature of the van der Waals interaction, especially for organic molecules.

Although the interfaces of organic molecules and silver halides are essential in the die sensitization of the photography, the mechanism is not fully understood at present. I expect the surface science technique will solve the problem and open a new field in opt-chemistry, and hopefully, in opt-electronics.

(ii) Microscopic nature of ferroelectricity.

There are many kinds of ferroelectric materials, but the mechanism was only studied phenomenologically in the sense of physics. Surfaces and interfaces of ferroelectrics will be useful to understand the microscopic nature of these materials.

(iii) Fabrication of new materials.

As demonstrated by van der Waals epitaxy, controlled crystal growth is a strong method to fabricate materials with novel physical properties.

The science of solid state materials will continuously increase in importance and that of hetero interfaces will be an essential part of this field.

REFERENCES

Chapter 1

1. J. A. Wilson and A.D. Yoffe: Adv. Phys. **18**, 193 (1969).

2a. P.A. Lee, G. Said, R. Davis, T.H. Lim: J. Phys. Chem. Solids **30**, 2719 (1969).

2b. A.Zunger and A.J. Freeman: Phys. Rev. **B16**, 906 (1977).

2c. R.B. Murray, A.D. Yoffe: J. Phys. **C5**, 738 (1972).

2d. A.Zungre and A.J. Freeman: Phys. Rev. **B17**, 1839 (1978).

2e. D.L. Greenaway, R. Nitsche: J. Phys. Chem. Solids. **26**, 1445 (1965).

2f. H. Isomäki, J. von Boehm: Phys. Lett. **A89**, 89(1982).

2g. D.W. Bullett: J. Phys. **C11**, 4501 (1978).

2h. R.A.Neville, B.L. Evans: Phys. Stat. Sol. **A13**, 483 (1972).

2i. R.V. Kasowski: Phys. Rev. Lett. **30**, 175 (1973).

2j. B.A. Parkinson: personal communication.

2k. B.L. Evans, R.A. Hazelwood: Phys. Stat. Sol. **A4**, 181 (1971) .

2l. D.J. Bradley, Y. Katayama, B.L. Evans: Solid State Commun. **11**, 1695 (1972).

2m. G. Domingo, R.S. Itoga, C. R. Kannewurf: Phys. Rev. **143** (1966) 536.

2n. P.A. Lee and G. Said: J. Phys. **D**(Ser 2), **1**, 837 (1968).

2o. S. Asanabe: J. Phys. Soc. Japan **16**, 1789 (1961).

2p. G. Busch, C. Frolich and F. Hulliger: Helv. Phys. Acta **34**,359 (1961).

2q. G. Domingo, R.S. Itoga and C.R. Kannewurf: Phys. Rev. **143**, 536 (1966).

2r. P. Buck: "IV-VI compounds" in *Preparation and Crystal Growth of Materials with Layered Structure*, Ed. R.M.A. Lieth, D. Reidel, Dordrecht, 1977, pp255-275.

2s. B.L.Evans: "Optical Properties of Layered Compounds", in *Optical and Electrical Properties*, Ed. P.A. Lee. , *Physics and chemistry of materials with layered structures*, Gen. Ed. E. Mooser, D. Reidel, Dordrecht, 1976, pp1-143.

2t. E. Doni and R. Girlanda: "Electronic Energy Bands", in *Electronic Structure*

and Electronic Transitions in Layered Materials, Ed. V. Grasso, in *Physics and chemistry of materials with low dimensional structures*, Gen. Ed. E. Mooser, D. Reidel, 1986, pp1-172.

3. A. Koma: Thin solid films **216**, 72 (1992); and references therein.

4. J.A. Wilson, F..J. Disalvo and S. Mahajan: Adv. Phys. **24**,117 (1975).

5. R.V.Coleman, B. Giambattista, P.K. Hansma, A. Johnson, W.W. McNairy and C.G. Slough: Adv. Phys. **37**, 559 (1988).

6a. R.V. Coleman, B. Drake, P.K. Hansma, G. Slough: Phys. Rev. Lett. **55**, 394 (1985).

6b. S.J. Hillenius and R.V. Coleman: Phys. Rev. **B18**, 3790 (1978).

6c. Di Salvo, F.J. Bagley, B.J. Voorhoeve and J.V. Waszczak: J. Phys. Chem. Solids, **34**,1357 (1973).

6d. F.J. Di Salvo, D.E. Moncton, J.A. Wilson and J.V. Waszczak: Phys. Rev. **B14**, 1543 (1976).

7. H. P. Hughes ad R.A. Pollak: Phil. Mag. **34**, 1025 (1976).

8. C. Liu, O. Singh, P. Joensen, A.E. Curzon and R.F. Frindt: Thin Solid Films, **113**, 165 (1984).

9. B. Palosz: Phys. Stat. Sol. **A77**, 11(1983); **A80**, 11(1983).

10. H. Baumhauer : Z. Krist. **50**, 33(1912).

11. S.Graezer: Schweiz Min. Pet. Mitt. **44**, 221 (1964).

12. R.M.A. Lieth and J.C.J.M. Terhell: *Preperation and Crystal Growth of Materials with Layered Structures*, Gen. Ed. F. Lévy, D.Reidel, Dordrecht, 1977, pp141-224.

13. E. Revolinsky, G.A. Siering and D.J. Beernsten: J. Phys. Chem. Solids **26**, 1029 (1965).

14. M. Kertesz and R. Hoffmann: J. Am. Chem. Soc. **106**, 3453 (1984).

15a. F.R. Gamble: J. Solid State Chem. **9**, 358 (1974).

15b. A. Madhukar: Solid State Commun. **16**,383 (1975).

16. F.C. Frank: Phil. Mag. **42**,1014 (1951).

17a. V.Vand and J.I.Hanoka: Mater. Res. Bull. **2**, 24 (1967).

17b. K.N. Rai: Phys. Stat. Sol. **A8**, 271 (1971).

17c. M. Dubey: Phys. Stat. Sol. **A29**, 213(1975)

17d. D. Kuhlmann-Wilsdorf, D. Pandey and P. Krishna: Phil. Mag. **A42** 527(1980).

18. R. Huisman, F. Kadjik and F. Jellinek: J. Less-common Metals **21**,187 (1970).

Chapter 3

1a. 小間・八木・塚田・青野編： 表面物性工学ハンドブック、丸善、1987.

1b. 塚田：仕事関数、共立出版、1983.

1c. R.G. Forbes, in *Scanning Tunneling Microscopy and related methods*, R.J. Behm et al. (eds.), Kluwer Academic Publishers, Dordrecht, 1990, pp163-172.

2a. N.D.Lang and W.Kohn: Phys.Rev. **B1**, 4555 (1970).

2b. N.D.Lang and W.Kohn: Phys.Rev. **B3**, 1215 (1971).

3. M.Hara, Y.Iwakabe, K.Tochigi, H.Sasabe, A.F.Garito, and A.Yamada: Nature **344**, 228 (1990).

4. W. Jaegermann: in *Photoelectrochemistry and Photovoltaics of Layered Semiconductors*, Ed. A. Aruchamy, Kluwer Academic Publishers, Dordrecht, 1992.

5. J.A. Wilson, F.J. Di Salvo and S. Mahajan: Adv. Phys. **24**,117 (1975).

6. G. Ertl, J. Küppers: *Low Energy Electrons and Surface Chemistry*, 2nd Edition, Chapter 4.3, (VCH Verlagsgesellschaft mbH, Weinheim, 1985).

7. V.Grasso (Ed.) : *Electronic Structure and Electronic Transitions in Layered Materials*, D.Reidel Publishing Company, Berlin, 1986.

8a. W. Jaegermann, C. Pettenkoffer, Ber. Bunzenges. Phys. Chem. **92**, 1354 (1988).

8b. M. Karamatos, C.A. Papageorgopoulos: Surf. Sci. **178**, 865 (1986).

8c. I.T. Mcgovern, R.H.Williams, C.H.B. Mee: Surf. Sci. **46**, 427 (1974).

8d. J.C. McMenamin, W.E. Spicer: Phys. Rev. **B16**, 5474 (1977).

8e. W. Jaegermann: Ber. Bunsenges. Phys. Chem. **92**, 537 (1988).

8f. R. B. Murray, R.H. Williams: Phil. Mag. **29**, 473 (1974).

8g. F.S. Ohuchi, W. Jaegermann, C. Pettenkofer, B.A. Parkinson: Langmuir **5**, 439 (1989).

8h. W. Jaegermann, F.S. Ohuchi, B.A. Parkinson: Surf. Sci. **201,** 211 (1988).

8i. S. Ledas, S. Kennou, M. S.D. Foulias, and C.A. Papageorgopoulos: Surf. Sci. **189/190**, 261 (1987).

8j. Th. Mayer, Pettenkofer, and W. Jaeferman in [4]

8k. W. Jaegermann, C. Pettenkofer, and B.A. Parkinson in [4].

8l. R.H. Williams, R.B. Murray, D.W. Goran, J.M. Thomas, E.L. Evans, J. Phys. C: Solid State Phys. **6**, 3631 (1973)

8m. *CRC Handbook of Chemistry and Physics*, 65th ed.,CRC press (1985), E-78.

9. N.V.Smith, S.D.Kevan, and F.J.DiSalvo: J. Phys. **C18** 3175 (1985).

10. W.A.Harrison: *Electronic Structure and the Property of Solids - The Physics of the Chemical Bond*, W.H.Freeman & Co., San Francisco,1980, Chapter 10.6.

11. R.A.Bromley,R.B.Murray and A.D.Yoffe: J.Phys. **C5**,759(1972).

12. D.W.Bullett: J.Phys. **C11**, 4501(1978)

13a. G.Wexler and A.M.Woolley: J.Phys. **C9**, 1185(1976).

13b. A.M.Woolley and G.Wexler: J.Phys. **C10**, 2601(1977).

14. J.A. Wilson and A.D. Yoffe: Adv. Phys. **18**, 193 (1965).

15. L.F.Matheiss: Phys.Rev. **B8**, 3719(1973).

Chapter 4

1. J.A. Wilson, F.J. Disalvo, and S. Mahajan: Adv. Phys. **23**, 117 (1974).

2. C. Liu, O. Singh, P. Joensen, A.E. Curzon and R.F. Frindt: Thin Solid Films, **113**, 165 (1984).

3. R.H.Friend and A.D.Yoffe: Adv. Phys. **36** ,1 (1987).

4. J.A.Wilson and A.D.Yoffe: Adv. Phys. **18**, 193 (1969).

5. T.Shimada, F.S.Ohuchi, and B.A.Parkinson: to be published.

6. H.P.Hughes and R.A.Pollak: Phil. Mag. **34**, 1025 (1976).

7. F.J.Di Salvo, B.J.Bagley, J.M.Voorhoeve, J.V.Waszczak: J.Phys.Chem.Solids **34**, 1357 (1973).

8. B.A. Parkinson: J. Am. Chem. Soc. **112**, 7498 (1990).

9. P.W.Williams: "Phase Transitions and Charge Density Waves in the Layered Transition Metal Dichalcogenides", in *Crystallography and Crystal Chemistry of Materials with Layered Structures*, Ed. by F. Lévy, D.Reidel, Dordrecht, 1976, pp51-92.

10. R.M.A.Lieth and J.C.J.M. Terhell: "Transition Metal Dichalcogenides" in Preparation and *Crystal Growth of Materials woth Layered Structures*, Ed. by R.M.A. Lieth, *Physics and Chemistry of Materials with Layered Structures*, Vol.1, D. Reidel, Dordrecht, pp186-189 ,1977.

11. F. Jellinek: J. Less Common Metals **4**, 9 (1962).

12. R.V.Coleman, B.Giambattista, P.K. Hansma, A.Johnson, W.W. McNairly, and C.G. Slough: Adv. Phys. **37**, 559 (1988).

13. M.Tanaka, W.Mizutani, N.Morita, S.Yamazaki, H.Bando, M.Ono, K.Kajimura: J. Microscopy (Part1) **152**, 183 (1988) .

14a. R.V. Coleman, B. Drake, P.K. Hansma, and C.G. Slough: Phys. Rev. Lett. **55**, 394 (1985).

14b. F. J. Di Salvo, D.E. Moncton, J.A. Wilson and J.V. Waszczak: Phys. Rev. **B14**, 1543 (1976).

14c. 三本木：伝導性低次元物質の化学、日本化学会編、学会出版センター、1983.

15. M.H.Hecht: Phys. Rev. **B41**, 7918 (1990).

16. N.J.Doran, G.Wexler and A.M.Wooley: J. Phys. **C11,** 2967 (1978).

17. X.L.Wu and C.M.Lieber: Phys. Rev. Lett. **64**, 1150 (1990).

18. E.H.Roderick, R.H.Williams, *Metal-Semiconductor Contacts* , 2nd Ed., Clarrendon Press, Oxford, 1988.

19. These substrates were not doped intentionally and the value for ρ was taken from the typical value in Table 3 in ref.4.

Chapter 5

1. M.A. van Hove and S.Y. Tong: *Surface Crystallography by LEED, Springer series in Chemical Physics* 2, Springer-Verlag, Berlin, 1979.

2. P. Hu and D.A. King: Nature **360**, 655 (1992).

3. S. Ino: Jpn. J. Appl. Phys. **16**, 891 (1977).

4a. A. Szöke: Proceedings of the Conference in Short Wavelength Coherent Radiation: Generation and Aplication, AIP Conf. Proc. No. 147, rd. by D.J. Attwood and J. Boker, AIP, New York, 1986. See also the references in chapter 8.

4b. D.K. Saldin, G.R. Harp, B.L. Chen and B.P. Tonner: Phys. Rev. **B44**, 2480 (1991).

5. R. Feidenhans'l: Surface Science Reports **10** (1989) 105.

6a. I.K. Robinson : *Handbook on Synchrotron Radiation*, Vol.3, Eds. by G. Brown and D.E. Moncton, Elsvier Science Publishers, Amsterdam, 1991.

6b. J. Als-Nielsen and H.Möhwald: *Handbook on Synchrotron Radiation*, Vol.4, Eds. by S. Ebashi, M. Koch and E. Rubensterin, Elsvier Science Publishers, Amsterdam, 1991.

7a. J.A. Wilson and A.D. Yoffe: *Adv. Phys.* **18** (1969) 193.

7b. R.M.A. Lieth and J.C.J.M. Terhell: *Preparation and Crystal Growth of Materials with Layered Structures*, Gen. ed. F. Lévy, D.Reidel, Dordrecht, 1977, p 141-224.

8. *International Tables for X-ray Crystallography*, vol III, Gen. Ed Kathleen Lonsdate, Kynoch Press (1952).

9. K. Ueno, T. Shimada, K. Saiki and A.Koma: Appl. Phys. Lett. **56** (1990) 327.

10. T. Matsushita, H. Maezawa, T. Ishikawa, M. Nomura, A.Nakagawa, A. Mikuni, Y. Muramatsu, Y. Satow, T. Kosuge, S. Sato, T. Koide, N. Kanaya, S.

Asaoka and I. Nagakura: Rev. Sci. Instrum. **60**, 1874 (1989).

11. T. Matsushita, A. Iida, K. Takeshita, K. Saito, S. Kuroda, H. Oyanagi, M.Sugi and Y. Furukawa: Jpn. J. of Appl. Phys. **30**, L1674 (1991).

12. R. Huisman, F. Kadjik and F. Jellinek: J. Less-Common Metals **21**, 187 (1970).

13a. W.O.Gillum, R.A.D. Wentworth and R.F. Childers: Inorg. Chem. **9**, 1825 (1970).

13b. M. Kertesz and R. Hoffman: J. Am. Chem. Soc. **106**, 3453 (1984).

14. M.A. Herman and H. Sitter: *Molecular Beam Epitaxy*, Springer Series in Materials Science 7, Springer-Verlag, Berlin, 1989, chapter 6.

Chapter 6

1. S.M. Sze: *Physics of Semiconductor Devices*, 2nd ed., John Wiley & Sons, New York, 1981, Chapter 11, 13, 14.

2. E.H. Rhoderick and R.H. Williams: *Metal Semiconductor Contacts*, 2nd ed., Clarendon Press, Oxford, 1988.

3. V. Heine: Phys. Rev. **A138**, 1689 (1965); Proc. Roy. Soc. **A331**, 307 (1972).

4a. R. Späh, U. Elrod, M. Lux-Steiner, E. Buchner and S. Wagner: Appl. Phys. Lett. **43**, 79 (1983).

4b. R. Späh, M. Lux-Steiner, M. Obergfell, E. Buchner and S. Wagner: Appl. Phys. Lett. **47**, 871 (1985).

5a. M.H. Hecht: J. Vac. Sci. &Technol. **B8**, 1018 (1990); Phys. Rev. **B41**, 7918 (1990).

5b. I.M.Vitominov, G.D.Waddill, C.M.Aldao, S.G. Anderson, C. Capaso and J.H. Weaver: Phys. Rev. **B40**, 3483 (1989).

5c. S.Chang, I.M. Vitomirov, L.J. Brillison, D.F. Rioux, P.D. Kirchner, G.F. Pettit, J.M. Woodall, M.H. Hecht: Phys. Rev. **B41**, 12299 (1990) .

6. V.P.Bhatt and K.Gireesan: J. Mater. Sci. Lett. **9**, 362 (1990).

7. D.Chun, R.M.Walser, R.W.Bené and T.H.Courtnoy: Appl. Phys. Lett. **24**, 479 (1974).

8. I.M.Catalano, A.Cingolani, A.Minafra and C.Paorici: Opt. Commun. **24**, 105 (1978).

9. A.Koma, K.Sunouchi and T.Miyajima: Microelectron. Eng. **2**, 129 (1984); J. Vac. Sci. & Technol. **B3**, 724, (1985).

10. T.Shimada, F.S.Ohuchi and B.A.Parkinson: J.Vac.Sci. & Technol. **A10**, 539 (1992).

11. T.Shimada, F.S.Ohuchi and B.A.Parkinson: to be published.

12. K.W.Nebesny, G.E.Collins, P.A.Lee, L.-K.Chau, J.Danziger, E.Osburn and N.R.Armstrong: Chem. Mater. **3**, 829 (1991).

13. B.A.Parkinson: J. Am. Chem. Soc. **112**, 7498 (1990).

14. R. Candia, B.S.Clausen and H.Topsoe: Bull. Soc. Chem. Belg. **90**, 1225 (1981).

15. W. Jaegermann: "Surface Studies of Layered Materials in Relation to Energy Converting Interfaces", in *Photoelectrochemistry and Photovoltaics of Layred Semiconductors*: Ed. By A. Aruchamy, Kluwer Acdemic Publishers, Dordrecht, 1992.

Chapter 7

1. J.A. Wilson, F.J. Di Salvo, and S. Mahajan: Adv. Phys. **23**, 117 (1974).

2a. H.P. Hughes and R.A. Pollak: Phil. Mag. **34**, 1025 (1976).

2b. G.K. Wertheim, F.J. Di Salvo and S. Chang: Phys. Rev. **B13**, 5476 (1976).

3a. G.D. Mahan: Phys. Rev. **163**, 612 (1967).

3b. P. Noziéres and C.T. De Dominics: Phys. Rev. **178**, 1097 (1969).

4a. V.L. Ginzburg: Phys. Lett. **13**, 102 (1964).

4b. D. Allender, J. Bray, J. Bardeen: Phys. Rev. **B7**, 1020 (1973).

5a. G. Scholz, P. Joensen, J.M. Reyes and R.F. Frindt: Physica **105B**, 214 (1981).

5b. W. Jaegermann, F.S. Ohuchi and B.A. Parkinson: Surf. Sci. **201**, 211 (1987).

6. F. S. Ohuchi et al: unpublished.

7. Cl. Ritter and R. Sxhöllhorn: Solid State Communications **61**, 117 (1987).

8. C. Pettenkofer, W. Jaegermann, B.A. Parkinson: Surf. Sci. **251/252**, 583 (1991).

9. N.V. Smith, S.D. Kevan and F.J. DiSalvo: J. Phys. **C18**, 3175.

10a. R.V.Coleman, B.Giambattista, P.K. Hansma, A.Johnson, W.W. McNairly, and C.G. Slough: Adv. Phys. **37**, 559 (1988).

10b. X.L.Wu and C.M.Lieber: Phys. Rev. Lett. **64**, 1150 (1990).

11. K. Sakamaki: PhD. thesis, Department of Chemical Energy Engineering, The University of Tokyo, 1991.

Chapter 8

1a. E.Evans and D.L.Mills: Phys. Rev. **B5**, 4126 (1972).

1b. E.Evans and D.L.Mills: Phys. Rev. **B7**, 853 (1973).

2. H. Raether: *Excitation of Plasmons and Interband Transitions by Electrons* , Springer Tracts in Modern Physics, Vol. 88, Springer Verlag, Berlin, 1980.

3. E. Tosatti and R. Girlanda: "Plasmons in Layered Materials" in *Electronic Structure and Electronic Transitions in Layered Materials*, Ed. by V. Grasso, D. Reidel, Dordrecht, 1986, pp461-492.

4. D. Pines: *Elementary Excitations in Solids*, W.A.Benjamin Press, New York, 1964, Chap. 3.

5. D.L.Mills: Surf. Sci. **48**, 54 (1975).

6a. H.-W.Drawin: Z.Phys. **164**, 513 (1961)

6b. H. Froitzheim: in *Electron Energy Loss Spectroscopy*, ed. H. Ibach, Springer-Verlag, Berlin 1977, pp 205-246.

7a. A. Stöke: *Proc. of Conf. on Short Wavelength Coherent Radiation: Generation and Application*, AIP Conf. Proc. No. 147, Ed. by D. J. Attwood and J. Boker,

AIP, New York, 1986.

7b. D.K.Saldin, G.R.Harp, B.L.Chen and B.P.Tonner: Phys. Rev. **B 44** , 2480 (1991).

8. J.J.Barton: Phys. Rev. Lett. **61**, 1356 (1988).

9. A. Koma and K. Enari: *Proc. 14th International Conf. of Physics of semiconductors, Edinburgh, 1978* , Inst. Phys. Conf. Ser. No.43, 1979.

10. J.A.Wilson and A.D.Yoffe: Adv. Phys. **18**, 193 (1969).

11. K. Horioka, H. Iwasaki, A. Ichimiya, S. Maruno, S.T. Li and S. Nakamura: Jpn. J. Appl. Phys. **21**, L189(1982).

12. C. Kittel: *Introduction to Solid State Physics*, 5th ed. , John-Wiley & Sons, New York, 1976, Chapter 9.

13. M.P. Sear: Surf. Sci. **24**, 357 (1971).

Chapter 9

1. J.J. Harris, B.A. Joyce and P. J. Dobson: Surf. Sci. **103**, L90 (1981).

2. J. M. van Hove, C.S. Lent, P.R. Pukite and P.I. Choen: J. Vac. Sci. & Technol. **B1**, 741 (1983).

3. T. Sakamoto, N.J. Kawai, T. Nakagawa, K. Ohta and T. Kojima: Appl. Phys. Lett. **47**, 617 (1985).

4. K. Ueno, T. Shimada, K. Saiki and A. Koma: Appl. Phys. Lett. **56**, 327 (1990).

5. J.A. Wilson and A. D.Yoffe: Adv. Phys. **18**, 193 (1969).

Chapter 10

1. T.Yao and S.Maekawa: J. Cryst. Growth **53**, 423 (1981).

2. A.Koma,K.Sunouchi, and T.Miyajima: J. Vac. Sci. Technol. **B3**, 724 (1985)

3. A.M.Patterson and J.O.Williams: J. Electronic Materials, **13**, 621 (1984).

4. *CRC Handbook of Chemistry and Physics*, 65th ed., CRC press (1985).

5. *GMELIN HANDBUCH der anorganischen chemie - Se ERG-A3*, Springer-Verlag (1981).

6. K.Hayashi and A.Kawamura: Mat. Res. Bull. **21**, 1405 (1986).

7. J.A.Wilson and A.D.Yoffe: Adv. Phys. **18**, 193 (1969).

8. V.P.Bhatt, K. Gireesan and G.R. Pandya.: J. Cryst. Growth **96**, 649 (1989).

9. R.M.A.Lieth (Ed): *Preparation and Crystal Growth of Materials with Layered Structures*, *Physics and Chemistry of Materials with Layered Structures, Vol. 1*, D. Reidel, Dordrecht, 1976.